Max-Planck-Institut für Meteorologie
Max Planck Institute for Meteorology

MAX-PLANCK-GESELLSCHAFT

Global oceanic heat and fresh water forcing datasets based on ERA-40 and ERA-15

Frank Röske

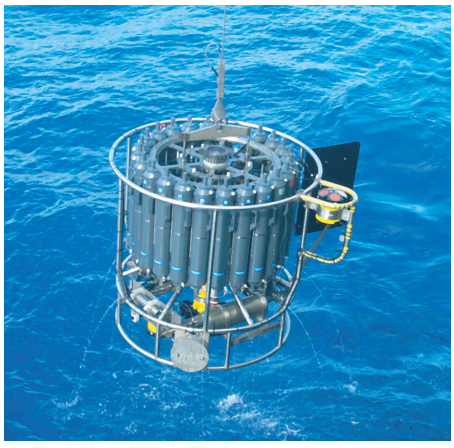

Berichte zur Erdsystemforschung 13/2005

Reports on Earth System Science

Hinweis

Die Berichte zur Erdsytemforschung werden vom Max-Planck-Institut für Meteorologie in Hamburg in unregelmäßiger Abfolge herausgegeben.

Sie enthalten wissenschaftliche und technische Beiträge, inklusive Dissertationen.

Die Beiträge geben nicht notwendigerweise die Auffassung des Instituts wieder.

Die "Berichte zur Erdsystemforschung" führen die vorherigen Reihen "Reports" und "Examensarbeiten" weiter.

Notice

The Reports on Earth System Science are published by the Max Planck Institute for Meteorology in Hamburg. They appear in irregular intervals.

They contain scientific and technical contributions, including Ph. D. theses.

The Reports do not necessarily reflect the opinion of the Institute.

The "Reports on Earth System Science" continue the former "Reports" and "Examensarbeiten" of the Max Planck Institute.

Anschrift / Address

Max-Planck-Institut für Meteorologie
Bundesstrasse 53
20146 Hamburg
Deutschland

Tel.: +49-(0)40-4 11 73-0
Fax: +49-(0)40-4 11 73-298
Web: www.mpimet.mpg.de

Layout:

Bettina Diallo, PR & Grafik

Titelfotos:
vorne:
Christian Klepp - Jochem Marotzke - Christian Klepp
hinten:
Clotilde Dubois - Christian Klepp - Katsumasa Tanaka

Berichte zur Erdsytemforschung 13/2005

Global oceanic heat and fresh water forcing datasets based on ERA-40 and ERA-15

Frank Röske

Hamburg 2005

Reports on Earth System Science 13/2005

ISSN 1614-1199

Frank Röske
Max-Planck-Institut für Meteorologie
Bundesstrasse 53
20146 Hamburg
Germany

ISSN 1614-1199

Global oceanic heat and fresh water forcing datasets based on ERA-40 and ERA-15

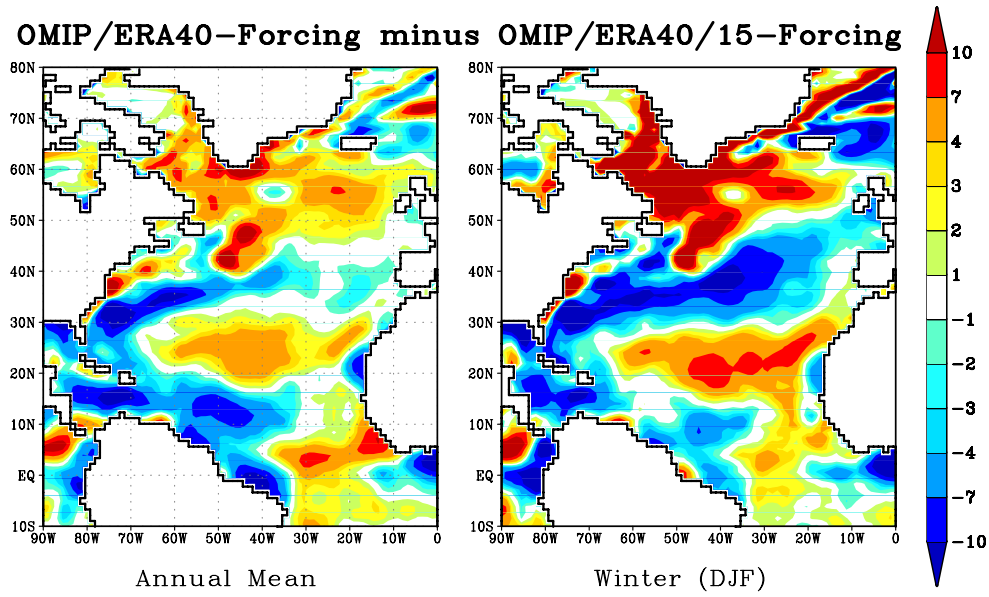

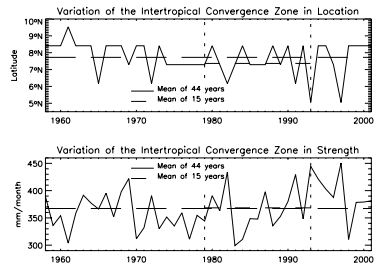

Frank Röske

Hamburg 2005

Contents

Abstract

A global heat and fresh water dataset based on the data of the second ECMWF Re-Analysis project (ERA-40) is presented that is constructed in the same way as the dataset based on the data of the first project (ERA-15) and can be used as surface boundary conditions for ocean models with sea ice components. The definition of these conditions is based on bulk formulae. A mean annual cycle on a daily basis was constructed from ERA-40 for all relevant parameters including wind stress. Continental runoff is considered by using a runoff model.

To estimate implied meridional oceanic heat transports and to avoid temporal drifts of globally averaged deep ocean temperature and salinity in ocean model simulations, the heat and fresh water budgets have been closed by applying an inverse procedure to fine-tune the fluxes towards observed transports. Winds and short wave radiation at Southern higher latitudes and short and long wave radiation in the subsidence zones are corrected. Applied to any ocean/sea-ice model, the forcing dataset would induce only a relative small net sea-surface buoyancy loss.

A comparison of both datasets shows that the effects of the changes in the assimilation system of ERA are larger than the effects due to the different periods. The latter effects reveal a southward shift of the Intertropical Convergence Zone (ITCZ) in time and a pattern in the difference of the net heat flux corresponding to a low phase of the North Atlantic Oscillation (NAO). This pattern is essentially determined by a similar pattern in the latent heat flux with a gradient across the North American basin of about 15 to 20 Wm^{-2} for the annual mean. That confirms that the first dataset is biased towards a NAO high phase whereas the second one covers a whole NAO period.

1 Introduction

A global heat and fresh water forcing dataset based on the ECMWF Re-Analyses (ERA-40; Simmons and Gibson, 2000) is presented which is the successor of a similar dataset based on ERA-15 (Gibson et al., 1997; Röske, 2006) (henceforth Röske (2006) will be referred to as ROM). These datasets have been developed for an Ocean Model Intercomparison Project (OMIP) in which the results of ocean models which are part of coupled atmosphere/ ocean/sea-ice models are assessed with respect to the model formulation. The ERA-40 data cover the time period from September 1957 to August 2002. For the forcing dataset, however, only complete years were used (44 years from 1958 to 2001). This dataset was constructed in the same way as the first one based on ERA-15. The main construction elements are summarized as follows.

The surface boundary conditions of the dataset are defined by using the net heat flux which is the sum of short and long wave radiation as well as of the turbulent, i.e. the sensible and latent heat fluxes. The turbulent heat fluxes are computed by using the bulk formulae of Kara et al. (2005). They adapted the formula to the Tropical Ocean Global Atmosphere Coupled Ocean-Atmosphere Response Experiment (TOGA COARE) algorithm version 3.0 (Fairall et al., 2003). For the dataset based on ERA-15, the bulk formulae of Kara et al. (2005) have been extended by a parameterization of sea ice concentration to enhance the turbulent heat loss in ice covered regions, which is underestimated by ERA-15 (ROM). For the ERA-40 based dataset presented in this report, the same extended bulk formulae are used.

For OMIP, it is crucial that the ocean models are treated in the same way. None of them is to be at an advantage or at a disadvantage. The forcing dataset must be the same for every model and may not be dependent on any property of the ocean models. It must be possible to test the dataset for its own properties independently of any ocean model. Thus, two cases must be distinguished: the case when the forcing dataset is regarded independently of any ocean/sea-ice model - the "no-ocean-model" case - and the case when the dataset is applied to force such models - the "ocean-model" case. In

this report, only the dataset is represented (the "no-ocean-model" case). However, additional information is presented about what has to be considered in the case when this dataset is used to force an ocean model (the "ocean-model" case).

The first information has to do with the bulk formulae. They contain the sea surface temperature (SST) and the sea ice concentration (SIC) as "interface" parameters. In the "no-ocean-model" case, SSTs from ERA are used and observed SICs from the National Snow and Ice Data Center (NSIDC; Comiso, 2002). In the "ocean-model" case, SSTs as computed by ocean models and also SICs, if these models contains prognostic sea-ice models, are to enter the formulae. Because of using bulk formulae and in order to avoid temporal drifts of globally averaged deep ocean temperature and salinity in the ocean models when they are driven by the dataset, the budgets of heat and fresh water should be closed. The imbalance, i.e. the integral of the net heat and fresh water flux over the whole globe and the time period given, should be small, i.e. within $\pm$ 1 Wm^{-2} and $\pm$ 1 mm/month, respectively.

The second information has to do with the closure of the heat and fresh water budgets. In this report, the closure is done independently of any ocean model. The results of the closure should be used in the "ocean-model" case. The German OMIP effort has shown that although the budgets were closed before the dataset was used to drive the ocean models, the resulting imbalances of the models were nearly in the range mentioned above (Table 1; Fritzsch et al., 2000).

Ocean model	heat flux	fresh water flux
MOM2	0.4	-0.6
HOPE	1.2	-1.4

Table 1: Global imbalances of the Modular Ocean Model version 2 (MOM2; Pacanowski, 1995) with coupled sea ice and parallelized code (Fritzsch et al., 1998) and of the Hamburg Ocean Primitive Equation model (HOPE; Wolff et al., 1997) after having been forced over 100 years, that means forced by a 100-fold application of the ERA-15 based climatological dataset. The numbers include effects of salinity relaxation and ice growth. Heat fluxes are in Wm^{-2} and fresh water fluxes in mm/month.

The ocean models used in the German OMIP effort differ in their formulation. If other ocean models were driven by this dataset it would be expected that also their imbalances are small. However, carefulness is necessary when the models are driven over more than 100 years. If they are driven over more than about 170 years, density changes of more than 1 kg m^{-3} would be induced in a surface layer of 10 m thickness.

The budgets of the dataset were closed by using the inverse procedure after Isemer et al. (1989) and da Silva et al. (1994). When the procedure was developed by Isemer et al. (1989), a linearization was performed. Therefore, the adjustment provided by this procedure to reach a global balance is "sufficiently small". For larger adjustments, however, regional corrections are performed, partly on the base of global schemes, which are independent of the inverse procedure.

An algorithm to construct a mean annual cycle on a daily basis (Röske, 2001) was applied which allows to study the mean oceanic circulation in the "ocean-model" case.

The forcing dataset based on ERA-40 is compared to a mean annual cycle derived from data of the National Centers for Environmental Prediction and National Center for Atmospheric Research (NCEP/NCAR) Re-Analyses (NRA; Kalnay et al., 1996) covering the same time period as ERA-40 (1958 to 2001), referred to as "NRA-40", and to the surface marine dataset of da Silva et al. (1994) derived from the Comprehensive Ocean Atmosphere Data Set (COADS; Woodruff et al., 1987) covering 45 years from 1945 to 1989.

To determine how much the mean annual cycles based on ERA-15 and ERA-40 will differ from each other, the average of those cycles is subtracted from one another and the difference is studied. However, the difference is influenced by changes in the assimilation system of ERA and by effects of the different periods, as well. If one is interested in the effects of only one of these influences independently from each other, both effects have to be separated.

This is accomplished by introducing another (third) climatological forcing dataset, in addition to those based on the 15 years of ERA-15 (the first

dataset) and based on the 44 years of ERA-40 (the second dataset). This third dataset again is based on ERA-40 but only on those data covering the ERA-15 time period, i.e. the years 1979 to 1993 (ERA-40/15). Also this forcing dataset is constructed in the same way as the other ones. Then, two differences can be computed. The "first" difference is the difference between the third forcing dataset (based on ERA-40/15) and the first one (based on ERA-15) representing the effect of the changes in the assimilation system of ERA and the "second" difference is the difference between the second forcing dataset (based on ERA-40) and the third one (based on ERA-40/15) representing the effect of the different periods (Table 2 in section 3.1).

To assess quantitatively how much of the main gain and loss regions of heat and fresh water is still being observed in the "first" and "second" differences, correlation coefficients between the fluxes and their differences are computed. For the "second" difference these coefficients are smaller than 0.1. Thus, the differences are independent of the fluxes and the main gain and loss regions of heat and fresh water are eliminated.

The "second" difference of the fresh water fluxes in the tropical Pacific Ocean shows a latitudinal band of negative values along the equator and a band of positive values north of it. This is supposed to be involved with a change of the Intertropical Convergence Zone (ITCZ) in strength and location comparing the ERA-40 period to the ERA-15 period.

To interpret the "second" difference of the heat fluxes in the North Atlantic Ocean, the North Atlantic Oscillation (NAO) is considered. The NAO index was anomalously low in the 1960s and anomalously high in the 1980s and 1990s (Wanner et al., 2001). Thus, the mean annual cycles of ERA-15 and of ERA-40/15 are biased towards the NAO high phase (NAO+), whereas the mean annual cycle of ERA-40 covers a whole NAO period, i.e. a NAO+ and a NAO low (NAO-) phase.

The NAO index is defined by the pressure difference between Iceland and Azores. During a high index (NAO+) anomalously warm SST over the North American Basin and anomalously cold SST situated east/southeast Greenland and west of North Africa are observed (Wanner et al., 2001). During

a low index (NAO-) the pattern regarding the SST anomalies is reversed. Henceforth, this pattern will be referred to as "tripole" pattern. The NAO is a winter phenomenon and therefore, the short wave radiation is small during that time. The long wave radiation of a black body and the turbulent heat fluxes are sensitive to the SST. Therefore, it is expected that the net heat flux of the difference between the datasets based on ERA-40 and on ERA-40/15 reflects the "tripole" pattern of NAO-.

This paper is organized as follows. The construction of the forcing dataset based on ERA-40 is described in section 2. The closure procedure is presented in section 3. The results of the comparison of the forcing datasets are given in section 4. Conclusions follow in section 5.

2 The forcing datasets

A short overview of the ERA-40 project is given. In ERA-40, a variational data assimilation system has been used to make a new synthesis of the in-situ and remotely-sensed measurements made since mid-1957 (satellite based since 1972), when a major improvement was made to the atmospheric observing system in preparation for the International Geophysical Year, 1958 (Simmons and Gibson, 2000). The data used in this study comprise 44 years from 1958 to 2001. They are available on a Gaussian grid with T106 truncation corresponding to a horizontal resolution of $1.125° \times 1.125°$.

For the first forcing dataset based on ERA-15, the 24-hourly forecast cycle was selected to become the basis of the dataset (ROM). In order to obtain maximum comparability to this dataset, also for the second forcing dataset based on ERA-40 the same forecast cycle was selected. From two forecasts per day (one 24 hour forecast begins at 0:00 UTC and one at 12:00 UTC) daily values were derived.

Net heat fluxes are calculated from net short wave radiation, net long wave radiation, and the turbulent, i.e. the sensible and latent heat fluxes. The turbulent heat fluxes are computed using bulk formulae (Kara et al., 2005; Appendix A). The input variables for these formulae are: 2 meter air

temperature T_a, 2 meter dew point temperature, freezing point temperature is represented as a function of salinity derived from the equation of state (UNESCO 1983; H. Simmons, pers. comm.), scalar wind V, mean sea level pressure p and the surface temperature T_s. The transfer coefficients in the bulk formulae are computed from T_a, T_s, V, p, and saturated specific humidity q_a as a function of T_a (Buck, 1981). The formulae are extended by a parameterization of sea ice concentration c_{ice}.

In this report, the forcing datasets are regarded independently of any ocean/sea-ice model. T_s is taken from ERA and c_{ice} are observed sea ice concentrations from the National Snow and Ice Data Center (NSIDC; Comiso, 2002). However, observed fractional sea ice concentrations ($0 < c_{ice} < 1$) are not available prior to 1979. Observed sea ice concentrations $c_{ice} = 0$ or $c_{ice} = 1$ prior to this year were not considered.

When the forcing datasets are applied to force ocean/sea-ice models, model simulations of T_s and c_{ice} should be used instead of ERA and observational data (the "ocean-model" case). Furthermore, if an ocean/sea-ice model simulates its own albedos, total short wave radiation Q_{sw}^{tot} including the reflected part is required instead of net radiation Q_{sw}^{net}. ERA provide only net radiation. Therefore, total radiation has to be computed. For this purpose, the albedo a of ERA was used in the following way:

$$Q_{sw}^{tot} = \frac{Q_{sw}^{net}}{(1-a)}. \tag{1}$$

In this report, net radiation Q_{sw}^{net} is used to calculate the heat budget independently of any ocean/sea-ice model.

For the long wave radiation, the same distinction of cases has to be made. If the forcing dataset is applied to any ocean/sea-ice model, the model SST can be considered in the following way:

$$Q_{lw,model} = Q_{lw,ERA} + \varepsilon\sigma(T_{s,ERA}^4 - T_{s,model}^4) \tag{2}$$

where $Q_{lw,model}$ is the long wave radiation in the ocean model, $T_{s,model}$ is the sea surface temperature of the model, $Q_{lw,ERA}$ is the net long wave radiation from ERA, $T_{s,ERA}$ is the sea surface temperature also from ERA, ε is the

emissivity of water, and $\sigma = 5.67 \cdot 10^{-8}$ $\mathrm{Wm^{-2}K^{-4}}$ is the Stefan-Boltzmann constant. Again, in this report, net radiation $Q_{lw,ERA}$ is used to calculate the heat budget independently of any ocean/sea-ice model.

For all relevant parameters a mean annual cycle has been produced. As for ERA-15, also for ERA-40, high-frequency variance shows its maximum in the year 1982, when a strong El Niño began (ROM).

Continental runoff is computed from continental precipitation (including snow) and evaporation by using the runoff model of ROM which is based on two datasets provided by Hagemann and Dümenil (1998). These datasets contain information about river catchment areas and main drainage basins globally.

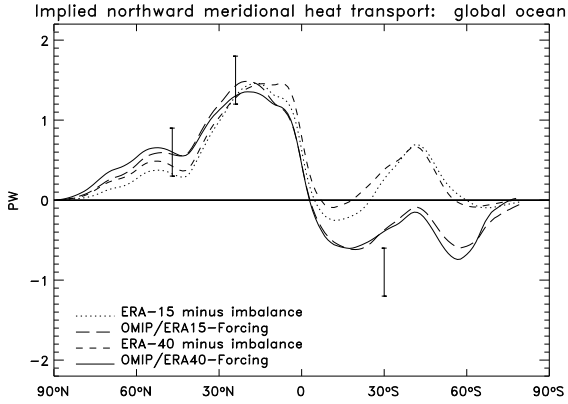

Figure 1: Implied meridional northward heat transports for the global ocean (Appendix D). The OMIP/ERA15- and OMIP/ERA40-Forcings are defined in section 3.1. Heat transport observations are from Macdonald and Wunsch (1996). Note that the x-axis starts at the North Pole.

Both, ERA-15 and ERA-40, show positive, i.e. northward directed implied meridional oceanic heat transports (MHTs; Appendix D) for the global ocean between 20°S and 60°S (Fig.1). Keith (1995) and Trenberth and Caron (2001) however, suggested southward directed heat transports. If the katabatic winds at Antarctica are corrected and short wave radiation is reduced in the Southern higher latitudes, then the MHTs between 20°S and 60°S

become negative, i.e. southward directed. The katabatic winds are not captured very accurately by the ECMWF analyses (Kim and Stössel, 1998; van den Broeke and van de Wal, 1997) and probably also not by ERA. They are corrected by using the global scheme from ROM (Appendix B). Short wave radiation is reduced by a simple multiplication with a constant factor between 60°S and 90°S and a smooth quadratic transition at 60°S. A factor of 0.89 for ERA-15 (ROM) showed best agreement with satellite observations from the Surface Radiation Budget (SRB). Because of the high similarity of the implied northward MHTs of ERA-15 and ERA-40 (Fig.1) the same factor was also applied on the short wave radiation from ERA-40.

Furthermore, to correct the bias of short and long wave radiation in areas of oceanic upwelling, the regions of subsidence, another global scheme from ROM (Appendix C) was applied.

3 Closure procedure

Meridional implied oceanic heat transports (Appendix D) can only be interpreted if the net heat flux has no imbalance, i.e. the integral of the heat flux over the whole globe and the time period given is close to zero. The imbalance of ERA-15 decreases with increasing length of the forecast period (Kallberg, 1997; Garnier et al., 2000). The mean annual cycle shows a similar behavior. For the 24-hour forecast cycle of the ERA-15 the imbalances of the heat and fresh water budget are minimal and small, i.e. within $\pm$ 1 Wm^{-2} and $\pm$ 1 mm/month, respectively (ROM). However, if bulk formulae are used to calculate the surface fluxes, the smallness of the imbalances and thus closed heat and fresh water budgets are not guaranteed any more. Then, a procedure for the closure is necessary. This holds also for ERA-40, where also (the same) bulk formulae are used.

For the closure of the heat and fresh water budgets of the mean annual cycle based on ERA-40 the same procedure was applied as used for the dataset based on ERA-15 (ROM). The closure is based on the inverse procedure after Isemer et al. (1989) and da Silva et al. (1994) to fine-tune the fluxes which

was applied on the daily data of the mean annual cycle. Tuning parameters $\mathbf{p}$ were computed by using $\mathbf{p} = 1 + \delta\mathbf{p}$ with the adjustment $\delta\mathbf{p}$ following equation (54) in da Silva et al. (1994):

$$\delta \mathrm{p} = (\mathrm{EA}^T(\mathrm{AEA}^T + \mathrm{R})^{-1}\mathrm{d}^* \tag{3}$$

with $\mathbf{E}$ is the covariance matrix for the errors of the tuning parameters $\mathbf{p}$, $\mathbf{A}$ the matrix of the sensitivities, i.e. of the changes of current transports $T(\phi, \mathbf{p})$ (Appendix D), with the current set of parameters $\mathbf{p}^*$, $\mathbf{R}$ the covariance matrix for the errors of the global heat transport estimates $\tilde{T}(\phi)$ derived from measurements made during ship cruises along latitudinal cross-sections, and $\mathbf{d}^*$ is the difference between those oceanographic estimates $\tilde{T}(\phi)$ and the transports $T(\phi, \mathbf{p}^*)$. As in ROM, global heat transport estimates after Macdonald and Wunsch (1996) were chosen, and zero heat and fresh water transports were prescribed at the Antarctic coast ($\tilde{T}(\phi_{Ac}) = 0$) However, in comparison of ERA-40 to ERA-15, the land sea mask has changed. In ERA-40, the Ross shelf is treated as land. Therefore, the latitude of those prescribed transports was shifted northward from $\phi_{Ac} = 80°\mathrm{S}$ to $\phi_{Ac} = 75°\mathrm{S}$.

3.1 Definition of "OMIP-Forcing"

To give the forcing datasets a name, the term "OMIP-Forcing" was chosen. The abbreviation "OMIP" (section 1) is used because the first dataset based on ERA-15 was developed to be used in such an intercomparison project of ocean models. Before the results of the application of the inverse procedure are presented, the term "OMIP-Forcing" is specified in regard to the main construction elements of the dataset presented thus far. This term includes the mean annual cycle based on ERA, the runoff model, the bulk formula after Kara et al. (2005) extended with a parameterization of sea ice concentration, the results of the inverse procedure after Isemer et al. (1989) and da Silva et al. (1994), the correction on the Southern Hemisphere, i.e. the global scheme for katabatic winds and the reduction of short wave radiation between 60°S and 90°S, and the correction of short and long wave radiation in the subsidence zones (section 2). This whole procedure was applied on

ERA-15, ERA-40, ERA-40/15, and on NRA-40, as well (Table 2). Regarding NRA-40, the correction on the Southern Hemisphere was not applied. However, another correction was applied on this dataset. Short wave radiation was reduced globally by a factor of 0.89 as suggested by Haak et al. (2003). There is no explanation, why this factor is the same as the one applied on short wave radiation from ERA-15 and ERA-40 on the Southern Hemisphere between 60°S and 90°S.

Dataset No.	based on	period	Dataset name
"first"	ERA-15	1979-1993	OMIP/ERA15-Forcing
"second"	ERA-40	1958-2001	OMIP/ERA40-Forcing
"third"	ERA-40/15	1979-1993	OMIP/ERA40/15-Forcing
	NRA-40	1958-2001	OMIP/NRA40-Forcing
Differences No.	Datasets involved		
"first"	"third" Dataset minus "first" Dataset		
"second"	"second" Dataset minus "third" Dataset		

Table 2: Overview of the datasets and the differences used.

Note that in this report the term "OMIP-Forcing" includes also the correction of short and long wave radiation in the subsidence zones, in contrast to the "OMIP-Forcing" which is referred to as the "final" one in Table 7 in ROM.

3.2 Results of the application of the inverse procedure

For the dataset based on ERA-15 as well as for the dataset based on ERA-40 two kinds of applications were designed. They were motivated from studying the effect of the correction on the Southern Hemisphere. Both applications are based on Equation (3) and there with the covariance matrix $\mathbf{R} = \mathrm{diag}(r_j^2)$ for the errors of the oceanographic heat transport estimates. For the r_j the error given by Macdonald and Wunsch (1996) (± 0.3 PW in each case) and a small error for the fresh water transport at 75°S were chosen. Large r_j mean small influence exerted by the oceanographic heat transport estimates on the inverse procedure (weak constraint), small r_j mean large influence

(strong constraint). The size of the r_j of Macdonald and Wunsch (1996) implies only a weak constraint.

The error r_j of the heat transport at 75°S is not known. If it is overestimated, i.e. if it is chosen to be large implying a weak constraint, and if the inverse procedure is performed without the correction on the Southern Hemisphere, an unrealistic large transport at this latitude is the result. However, this heat transport almost vanishes, when the correction is added on the fine-tuned data. This application is denoted as "only F" in Table 3.

Applications:	Correction Parameters p_i						Figure No.
	sw	lw	se	la	pr	ru	
ERA-40							
Strong only at 75°S (only F)	0.8947	1.0976	1.1465	0.9618	0.7189	0.9726	2 (a)
Strong only at 75°S (H & F)	0.9010	1.0980	1.1603	0.9722	0.7294	0.9736	3
ERA-40/15							
Strong only at 75°S (only F)	0.8855	1.0977	1.1326	0.9453	0.6923	0.9680	2 (a1)
NRA-40							
Strong only at 75°S (H & F)	0.8023	1.1804	1.1238	0.9303	0.5907	0.9757	
Strong only at 75°S (H & F) & Q_{sw}: -11% globally	0.8724	1.1562	1.1103	0.8834	0.5581	0.9737	2 (a2)
Allowed range:	0.9 - 1.1		0.8 - 1.2		0.5 - 1.5		

Table 3: Corrections parameters as suggested by the inverse procedure. 4 digits are necessary for an accuracy of 0.01 PW of the MHT especially on the Southern Hemisphere. "Strong" means: the heat (H) and fresh water (F) transport estimates have strong influence in the inverse procedure.

The applications "only F" yield non-vanishing MHTs at 75°S. They are reduced to approx. zero by using a correction for the (katabatic) winds and reducing Q_{sw} by 11% at 60°S - 90°S. The application "H & F" includes this correction for the ERA application but not for the NRA applications.

sw: Short wave solar radiation
lw: Long wave radiation
se: Sensible heat flux
la: Latent heat flux
pr: Precipitation
ru: Continental Runoff

However, this kind of application produces errors in the fresh water trans-

ports. Therefore, another kind of application was performed by choosing the error r_j of the heat transport at 75°S to be small and by including the correction on the Southern Hemisphere in the inverse procedure. This application is denoted as "H & F" in Table 3. Although the application on the dataset based on NRA-40 is also denoted with "H & F", the corrections on the Southern Hemisphere were not applied on this dataset. Regarding ERA, errors in the fresh transports are removed by this kind of application and buoyancy gains and losses can be estimated correctly.

Density fluxes D are derived from buoyancy B (Appendix E) with $D = B \cdot \rho/g$ and ρ is the density of water according to the equation of state (UNESCO, 1983) and $g = 9.8\text{m s}^{-2}$ the gravitational constant. Assuming a surface layer of a thickness of 10 m following Garnier et al. (2000), the OMIP/ERA40-Forcing including the bulk formulae and the results of the inverse procedure (Application "H & F") would induce a corresponding buoyancy loss of only 0.006 kg m^{-3} per year.

3.3 Comparison of the meridional transports

The implied meridional oceanic heat transports (Appendix D) of the OMIP/ ERA40-Forcing and the OMIP/ERA40/15-Forcing are rather similar (Fig.2 (a1 - e1)). However, they show some differences in comparison to the OMIP/ ERA15-Forcing. In the Northern higher latitudes, where the global ocean consists only of the Atlantic and Arctic Oceans, the northward heat transports of the OMIP/ERA40-Forcing are higher than those of the OMIP/ ERA15-Forcing (Fig.2(a1, b1)). The southward global heat transports of the OMIP/ERA40-Forcing in the Southern higher latitudes (at about 60°S) are stronger than those of the OMIP/ERA15-Forcing, too. The northward global heat transports of the OMIP/ERA40-Forcing are weaker in the Northern subtropics due to weaker heat transports in the North Pacific (Fig.2(a1, c1)). The order of magnitude of all these differences is about 0.1 PW.

Regarding the Southern subtropics, the northward heat transports of the OMIP/ERA40-Forcing in the South Atlantic are smaller than those of the OMIP/ERA15-Forcing and agree better with heat transport observations

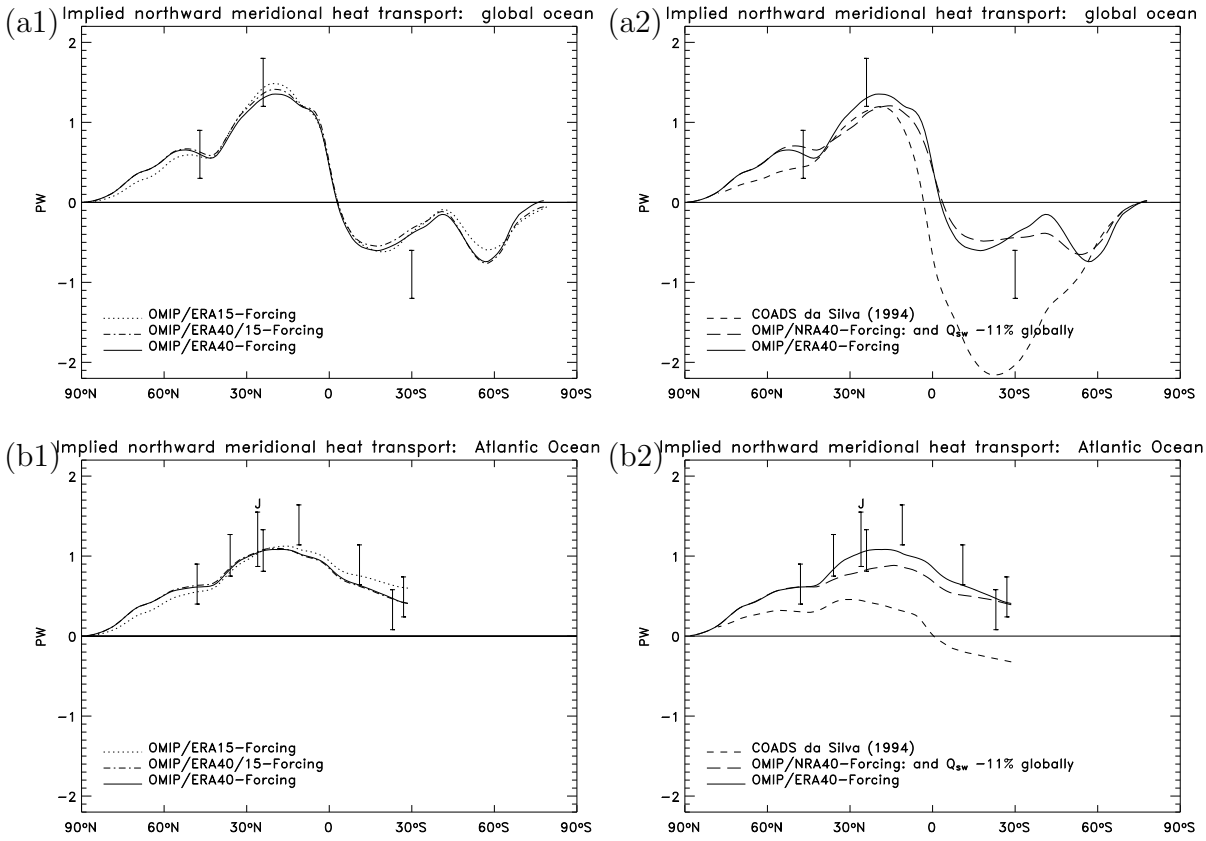

Figure 2: Implied meridional northward heat transports for the (a) global ocean, (b) Atlantic Ocean, (c) Pacific Ocean, and (d) Indian Ocean, and (e) Pacific and Indian Ocean combined. The left column (a1 - e1) shows the three OMIP-Forcings based on ERA-15, ERA-40, and ERA-40/15. In the right column (a2 - e2) the OMIP/ERA40-Forcing is compared to other climatologies. In both columns, this dataset is represented by solid lines. J denotes observed heat transport after Johns et al. (1997) (b1 and b2). M denotes observed heat transport after Macdonald (1993) (e1 and e2). All other heat transport observations are from Macdonald and Wunsch (1996). Note that the x-axis starts at the North Pole.

(Fig.2(b1)). Also, in the South Pacific, the southward heat transports of the OMIP/ERA40-Forcing are smaller than those of the OMIP/ERA15-Forcing (Fig.2(c1)). Because this difference is of similar order of magnitude as the

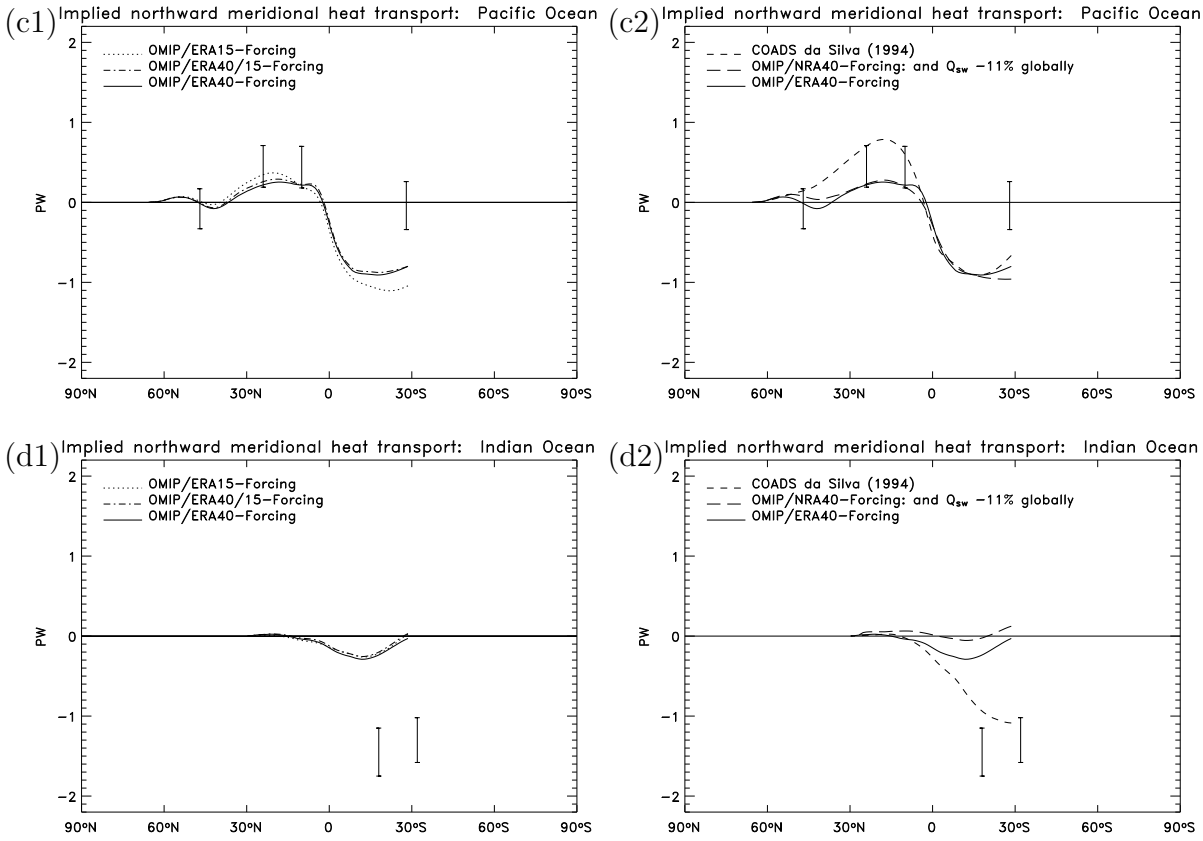

Figure 2: continued.

difference in the South Atlantic, the global heat transports of these datasets show almost no difference (Fig.2(a1)).

The differences between the implied meridional heat transports of the OMIP/ERA40-Forcing and of the OMIP/ERA40/15-Forcing are smaller than the differences between the transports of the OMIP/ERA40/15-Forcing and of the OMIP/ERA15-Forcing. That means, the effects of the different periods (section 4.2) are smaller than the effects of the changes in the assimilation system of ERA (section 4.1).

In comparison of the implied MHTs of the OMIP/ERA40-Forcing to those of the OMIP/NRA40-Forcing, a remarkable agreement of these datasets is

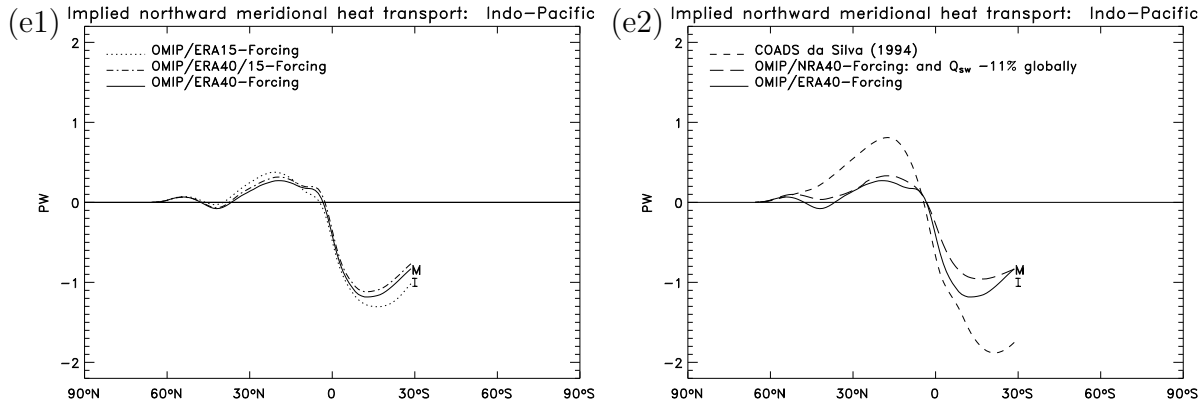

Figure 2: continued.

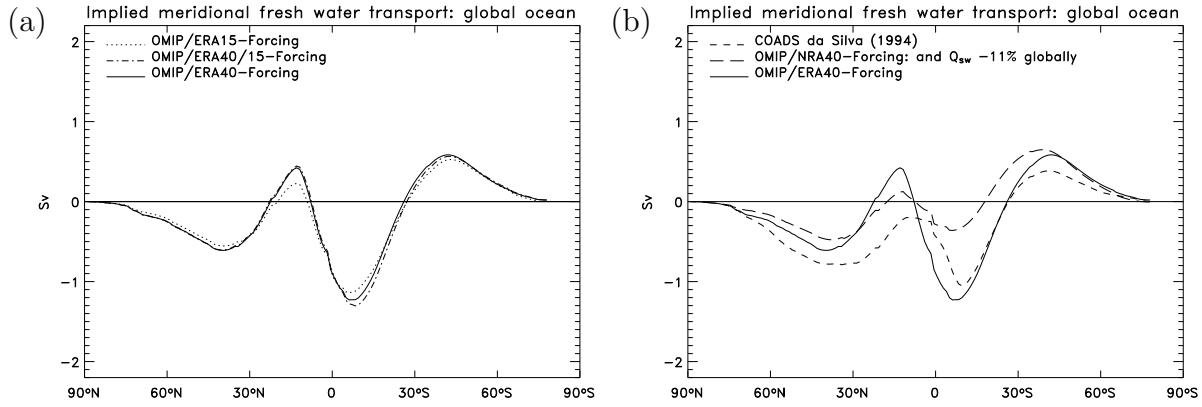

Figure 3: Implied meridional northward fresh water transports for the global ocean. For the OMIP-Forcing an additional inverse procedure (IP) was performed: strong constraints at 75°S for both heat and fresh water.

observed in the Northern higher latitudes globally and also in the midlatitudes in the North Atlantic Ocean (Fig.2(a2 and b2)). A good agreement of those datasets is also observed in the tropical and subtropical Pacific Ocean (Fig.2(c2)).

The OMIP/ERA40-Forcing dataset was also compared to the dataset of da Silva et al. (1994) based on COADS (Woodruff et al., 1987). The heat

budget of the da Silva dataset was closed by removing the global imbalance from the net heat flux. The heat transports as suggested by the closed dataset are smaller in the North Atlantic Ocean than estimated heat transports at certain latitudes (Fig.2(b2)). However, Grist and Josey (2003) showed that it is possible to derive MHTs from COADS release 1a (Woodruff et al., 1993) which are in agreement with most of the observed heat transports in the North Atlantic and even with the observed heat transport of Macdonald and Wunsch (1996) at 30°S globally (ROM).

For the OMIP/ERA15-Forcing, a disagreement between the implied heat transports of this dataset and the heat transport observations in the South Pacific and South Indian Oceans was observed which results from ignoring the Indonesian throughflow in computing the implied transports (ROM). The same disagreement was also observed for the OMIP/ERA40-Forcing. When the transports were computed for the OMIP/ERA15-Forcing from the Pacific and Indian Ocean combined, they agree very well with the heat transport observed at 30°S (Macdonald, 1993). (Fig.2(e2)). However, for the OMIP/ERA40-Forcing this agreement is only relatively good because the heat transport observation is less representative for the ERA-40 period.

For the OMIP/ERA15-Forcing, the systematic disagreement with the observed transports in each basin alone was utilized to estimate the heat transport through Indonesia by comparing the MHTs which were computed in each basin alone at the latitude of the Banda Strait (10°S; ROM). This was done also for the OMIP/ERA40-Forcing (Table 4).

Climatology:	ERA-40	NRA-40	OF40	OF40/15	da Silva
Heat transport:	0.4	0.5	0.6	0.6	0.2

Table 4: The heat transport in the Indonesian throughflow estimated by the difference of the implied meridional heat transports calculated in the Indian and Pacific Ocean separately at 10°S. Transports are in PW (10^{15}W). OF40: OMIP/ERA40-Forcing. OF40/15: OMIP/ERA40/15-Forcing.

Also the heat transport of this dataset in the Indonesian throughflow is consistent with the range estimated by Lebedev and Yaremchuk (2000), but it is somewhat smaller than the transport of the OMIP/ERA15-Forcing

(0.7 PW; ROM) indicating possibly a trend in the transport. However, the transports of the OMIP/ERA40/15-Forcing and of the OMIP/ERA40-Forcing are the same. Therefore, that difference is only an effect of the changes in the assimilation system of ERA.

3.4 Assessment of the subtraction of the forcing datasets

Regarding the two-dimensional distribution of the net surface fluxes, the regions of annual net heat gain and loss (Fig.4(a)) and of annual net fresh water gain and loss (Fig.4(b)) of the OMIP/ERA40-Forcing are in principle the same as those of the OMIP/ERA15-Forcing (ROM). The correlation coefficients between the fluxes of these datasets are larger than 90%. Especially the coefficient between the fluxes of only the two ERA-40 based datasets is almost 100% (Table 5).

Heat fluxes	OF15	OF40/15	"first" diff.	"second" diff.
OF15			0.05	-0.04
OF40/15	0.93		0.42	-0.03
OF40	0.92	0.99	0.42	0.10
Fresh water fluxes				
OF15			-0.04	-0.04
OF40/15	0.92		-0.04	0.05
OF40	0.92	1.00	-0.04	0.05

Table 5: Correlation coefficients between the fluxes of the forcing datasets and their differences. "First" diff.: OF40/15 minus OF15 (Table 2). "Second" diff.: OF40 minus OF40/15. OF15: OMIP/ERA15-Forcing. OF40/15: OMIP/ERA40/15-Forcing. OF40: OMIP/ERA40-Forcing.

The correlation coefficients between the heat fluxes of the "first" difference (Table 2) and those of the ERA-40 based datasets are 42%. In all other cases, the coefficients are $\leq 10\%$. Thus, by forming the "second" difference, i.e. the difference between the OMIP/ERA40-Forcing and the OMIP/ERA40/15-Forcing from the annual mean net heat and fresh water fluxes, the regions of annual net gain and loss of heat and fresh water are eliminated.

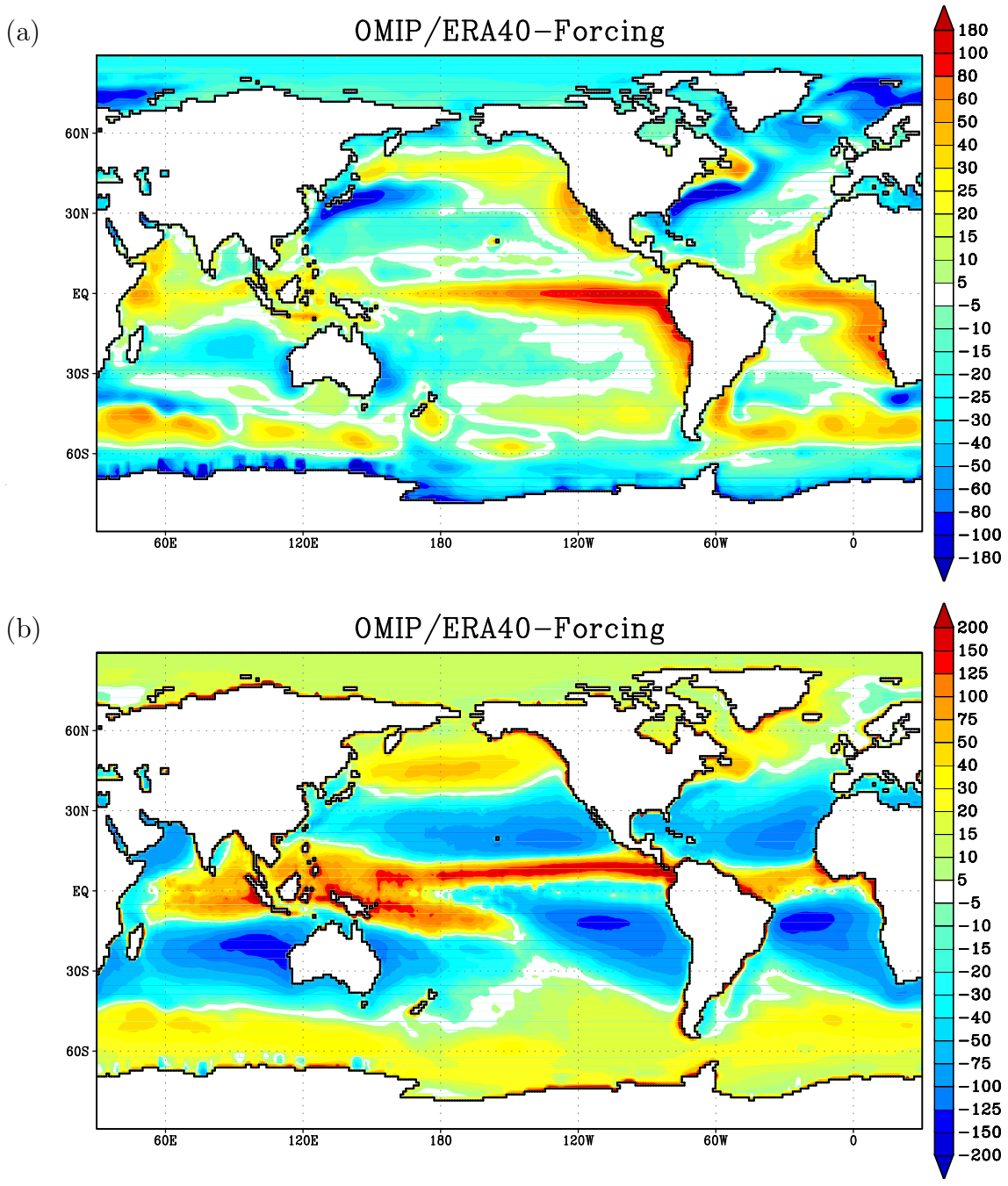

Figure 4: Annual mean distribution of (a) the net heat flux (in W/m^2) and (b) the net fresh water flux (in mm/month) from the OMIP/ERA40-Forcing.

4 Comparison of the "OMIP-Forcing" datasets

4.1 Effects of the changes in the assimilation system

In this section, the "first" difference (Table 2), i.e. the difference between the OMIP/ERA40/15-Forcing and the OMIP/ERA15-Forcing, representing the effects of the changes in the assimilation system of ERA, is examined in more detail.

The implied meridional oceanic heat transports (MHTs; Appendix D) of these two datasets are relatively similar except for the higher latitudes, where the MHTs of the former dataset are stronger than those of the latter dataset (Fig.2(a1) in section 3.3). Also, the zonally averaged net heat flux of these datasets from which the MHTs were derived are relatively similar except for the higher latitudes (Fig.5(e)). However, regarding short wave radiation and the absolute values of the latent heat flux in the tropics and subtropics, the OMIP/ERA40/15-Forcing is larger than the OMIP/ERA15-Forcing and closer to the da Silva dataset (Fig.5(a)). (Fig.5(d)). Considering the sign of these increases, they seem to balance each other.

Regarding the net heat fluxes in the Northern midlatitudes, there is a remarkable agreement of these two forcing datasets with the da Silva dataset (Fig.5(e)). In this region, long wave radiation of the OMIP/ERA40/15-Forcing agrees well with observation of the da Silva dataset (Fig.5(b)).

In the higher latitudes, the absolute value of the net heat flux, i.e. the net heat loss, of the OMIP/ERA40/15-Forcing is larger than that of the OMIP/ERA15-Forcing (Fig.5(e)) which is an effect of less short wave radiation (Fig.5(a)) and of larger sensible heat flux especially on the Southern Hemisphere (Fig.5(c)).

The precipitation peak of the OMIP/ERA15-Forcing in the tropics representing the Intertropical Convergence Zone (ITCZ) agrees well with the peak of the da Silva dataset (Fig.5(f)). However, the peak of the OMIP/ERA40/15-Forcing is higher than these peaks indicating an overestimation of precipitation in ERA-40 in this region (Hagemann et al., 2005).

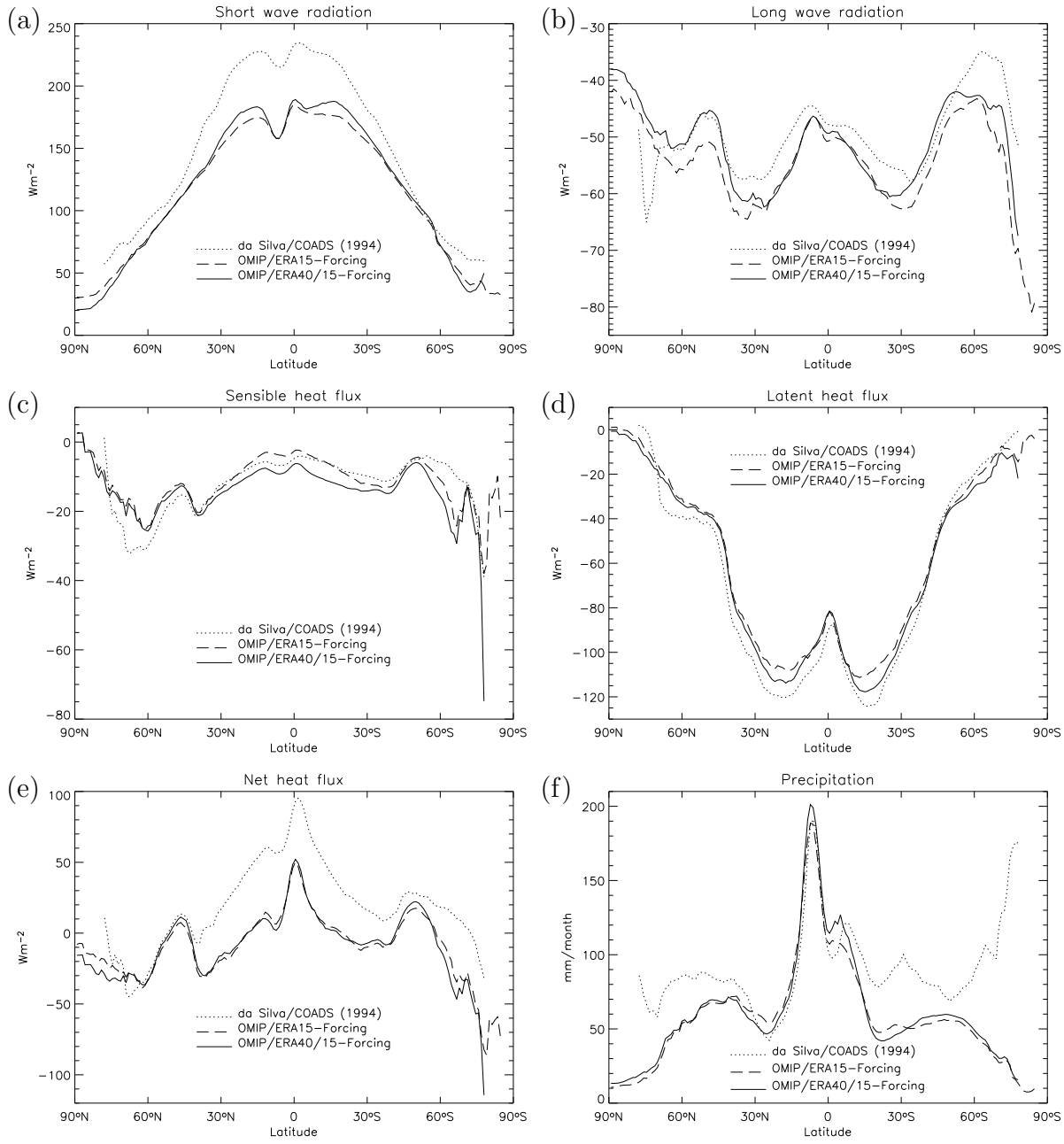

Figure 5: Zonally averaged annual mean flux components, (a) short wave radiation, (b) long wave radiation, (c) sensible heat flux, (d) latent heat flux, and (e) net heat flux (in Wm^{-2}) and (f) precipitation (in mm/month).

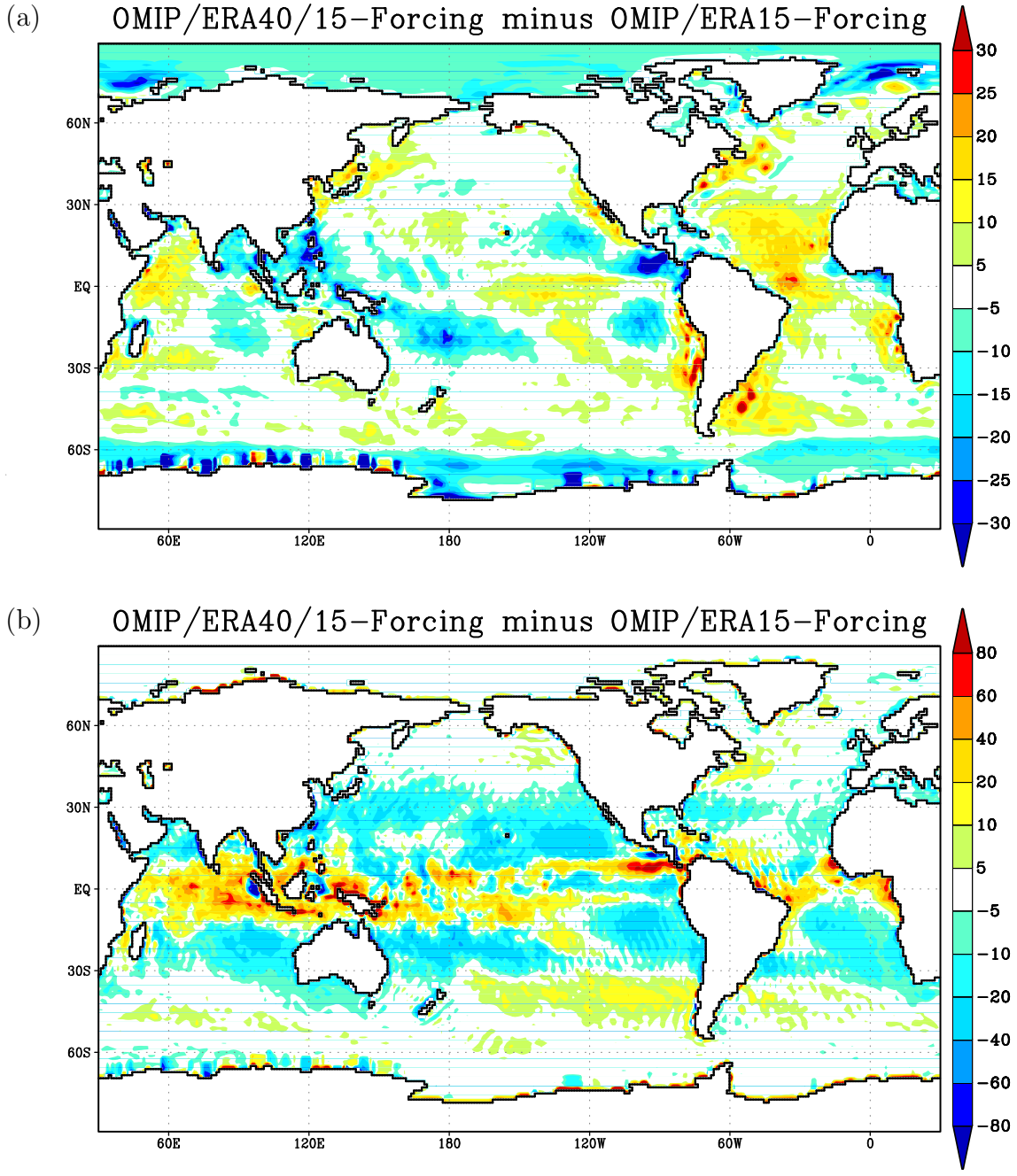

Figure 6: Difference between the mean annual distributions of the OMIP/ ERA40/15-Forcing and of the OMIP/ERA15-Forcing in (a) the net heat flux (in W/m^2) and (b) the net fresh water flux (in mm/month).

The smaller precipitation peak at about 5°S representing the South Pacific Convergence Zone (SPCZ) is in fairly good agreement with observations from the da Silva dataset, at least in magnitude.

In contrast to the zonal averages, the distribution of the difference between these datasets (the "first" difference), however, reveals regional biases (Fig.6). The difference in the net heat flux of these datasets (Fig.6(a)) is positive in the tropical Atlantic Ocean, the subtropical North Atlantic, the tropical central Pacific Ocean, the tropical West Indian Ocean, the subsidence zones, and the regions of the western boundary currents and the Brasil Current at about 10 to 20 (partly 30) Wm^{-2}. In the western Pacific warm pool, the SPCZ, and the Eastern tropical Pacific Ocean, the difference is negative at similar magnitude. The distribution of the difference in the fresh water flux (Fig.6(b)) reveals negative values of about 10 to 20 mm/month in the subtropics and positive values of similar magnitude in the region of the North Atlantic Current and in the midlatitudinal South Pacific and positive values up to 80 mm/month in the tropics.

4.2 Effects of the different periods

In this section, the "second" difference (Table 2), i.e. the difference between the OMIP/ERA40-Forcing and the OMIP/ERA40/15-Forcing representing the effects of the different periods, is examined.

The "second" difference is shown with the same scale (Fig.7) as the "first" difference (Fig.6) confirming the conclusion in section 3.3 that the effects of the different periods are smaller than the effects of the changes in the assimilation system of ERA.

4.2.1 Fresh water flux

The "second" difference of the fresh water flux reveals negative values (10 to 20 mm/month) mainly in the tropical Pacific Ocean and the Gulf of Mexico (Fig.7(a)). Positive values of similar magnitude are observed in parts of the subtropics, up to 40 mm/month in the tropical Pacific Ocean along the ITCZ and in the tropical Atlantic Ocean and up to 60 mm/month in the western Pacific warm pool.

In the tropical Pacific Ocean, a latitudinal band of negative values is observed along the equator and a band of positive values north of it. This might have to do with a change of the ITCZ in strength and location. To analyse this effect, a rectangular box was formed (Fig.7(a)). In this box, the net fresh water fluxes were averaged zonally. The maximum of these zonal averages was determined in strength and location for each year of ERA-40 (Fig.8). The strengths averaged over the periods of ERA-15 and ERA-40 do not differ much from each other. However, the location averaged over the ERA-15 period is about 0.4° farther south than the location averaged over the ERA-40 period. The northernmost location occured in 1961, the southernmost locations in 1993 and 1997.

4.2.2 Heat flux

The "second" difference in the net heat flux is in the range $\pm$ 5 Wm^{-2} almost everywhere except for some small spots distributed over the globe (Fig.7(b)).

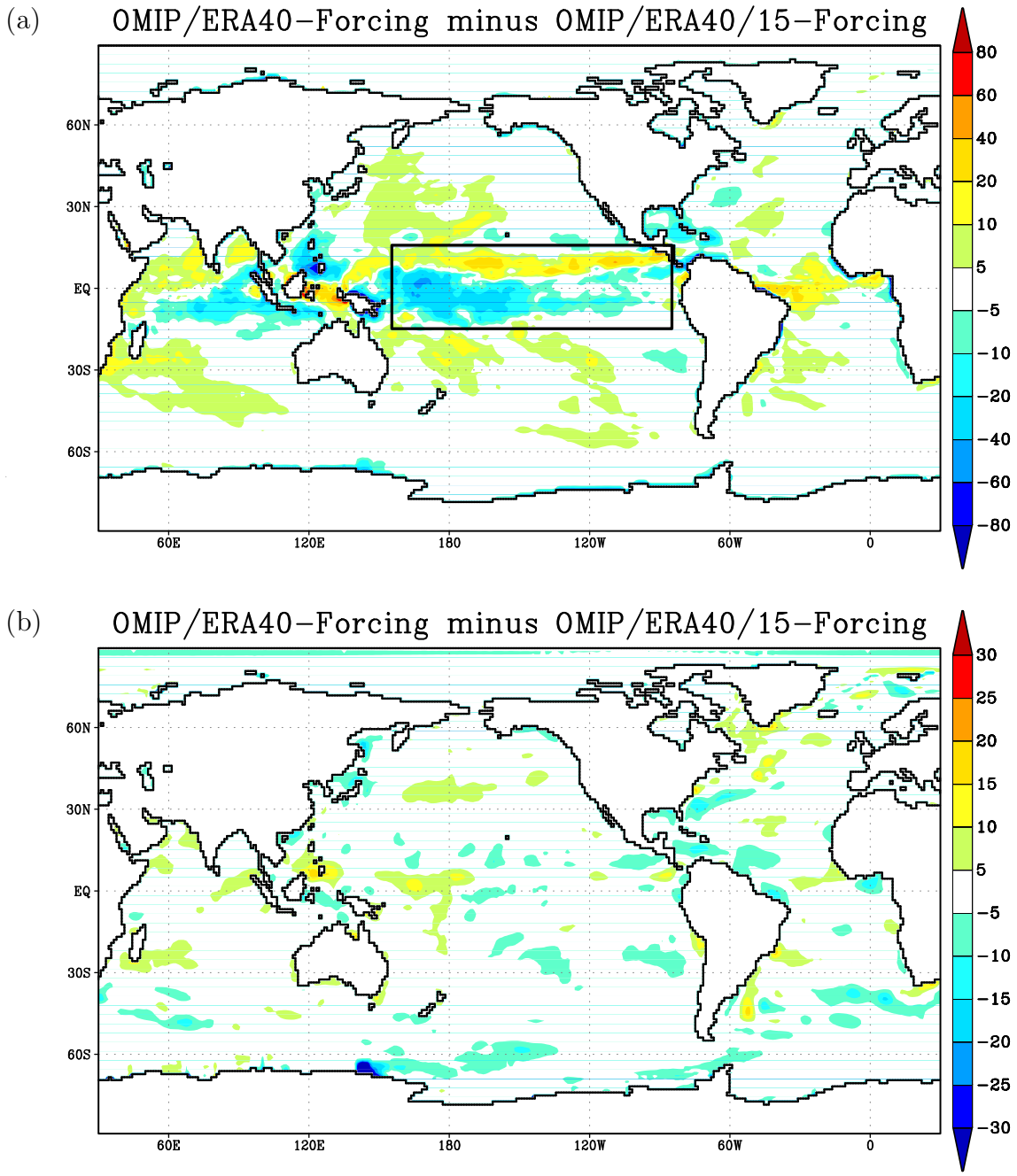

Figure 7: Annual mean distribution of the difference between the OMIP/ERA40-Forcing and the OMIP/ERA40/15-Forcing (the "second" difference) for (a) the net fresh water flux (in mm/month) and (b) the net heat flux (in W/m^2). The box in (a): 16°N, 14°S, 155°E, 85°W. Note the different scale in the North Atlantic Ocean in comparison to Fig.9(a).

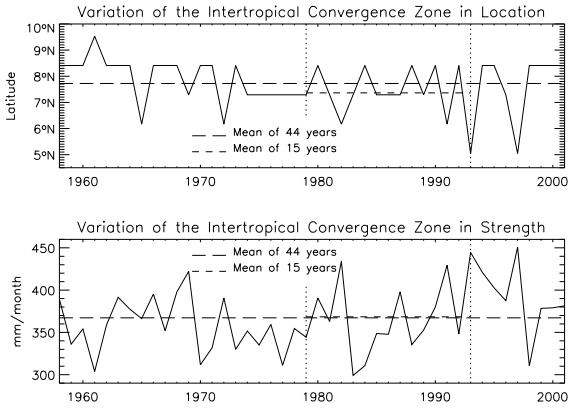

Figure 8: Location and strength of the maximum of the zonally averaged fresh water flux in the box of (Fig.7(a)) for the "second" difference (Table 2).
Mean of 44 years: 367 mm/month, 7.72°N.
Mean of 15 years: 368 mm/month, 7.36°N.

For a better interpretation of this difference it is shown again using a refined scale (Fig.9(a)). A tripole pattern is observed in the North Atlantic which can be interpreted as a low phase of the North Atlantic Oscillation (NAO) (section 1). This pattern is more distinct when the fluxes are averaged only over the winter months December, January, and February (Fig.9(a), right panel).

The difference of the net heat flux across the North American Basin is about 15 to 20 Wm^{-2} for the annual mean and more than 20 Wm^{-2} in winter. Looking at the components of the net heat flux, the "second" difference in the sensible heat flux does not show a tripole pattern (Fig.9(c)). The "second" difference in the long wave radiation seems to show the tripole only in winter. In this season it has a gradient of about 5 Wm^{-2} (Fig.9(b)). The main contributor to the gradient in the net heat flux, however, is the latent heat flux (Fig.9(d)). The corresponding gradient across the North American Basin is about 15 to 20 Wm^{-2} for the annual mean and about 20 Wm^{-2} in winter.

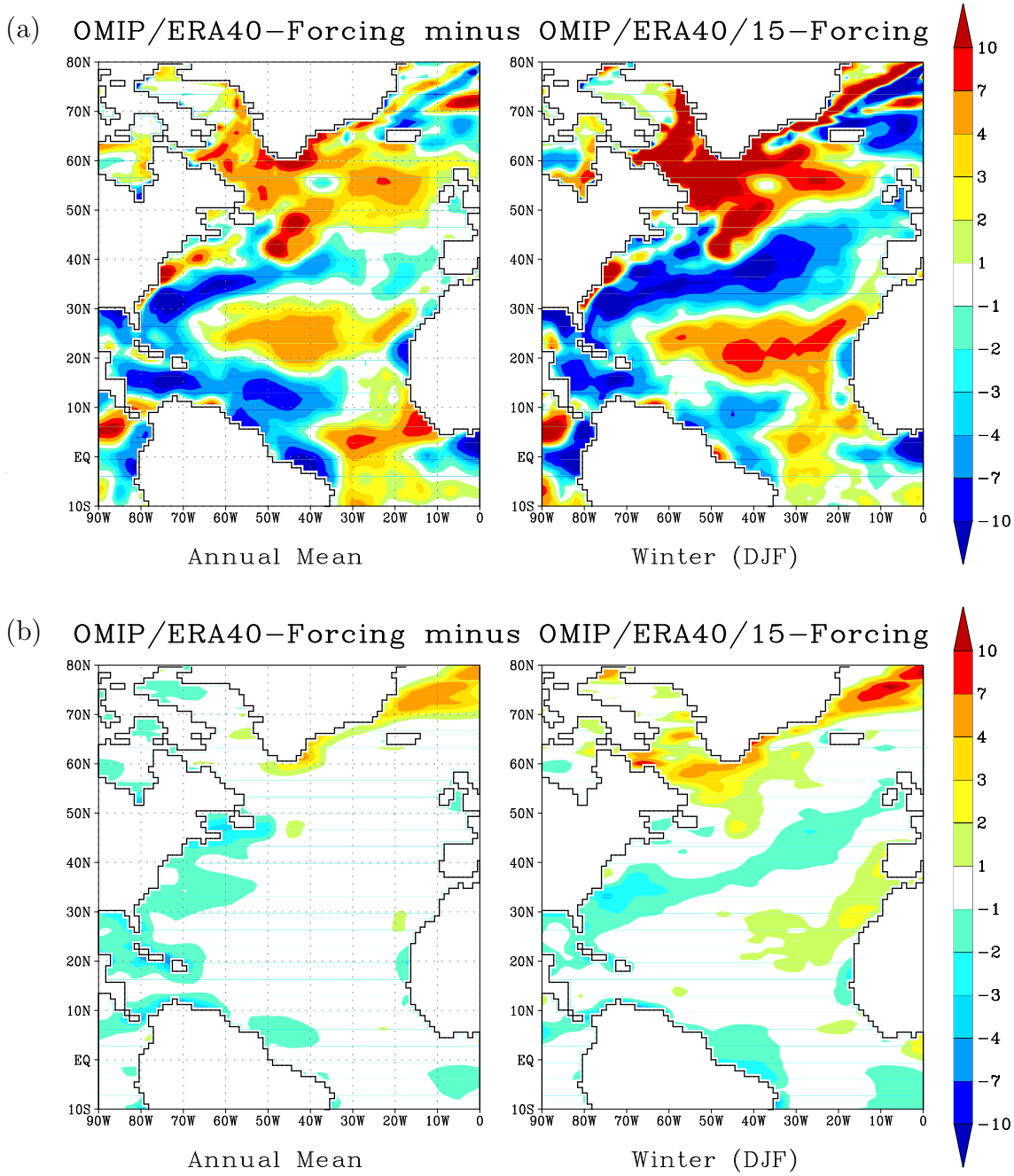

Figure 9: Annual mean (left) and winter mean flux distribution (right) of the difference between the OMIP/ERA40-Forcing and the OMIP/ERA40/15-Forcing (the "second" difference) for (a) the net heat flux, (b) the long wave radiative flux, (c) the sensible heat flux, and (d) the latent heat flux (in W/m^2). Note the different scale for the net heat flux in comparison to Fig.7(b).

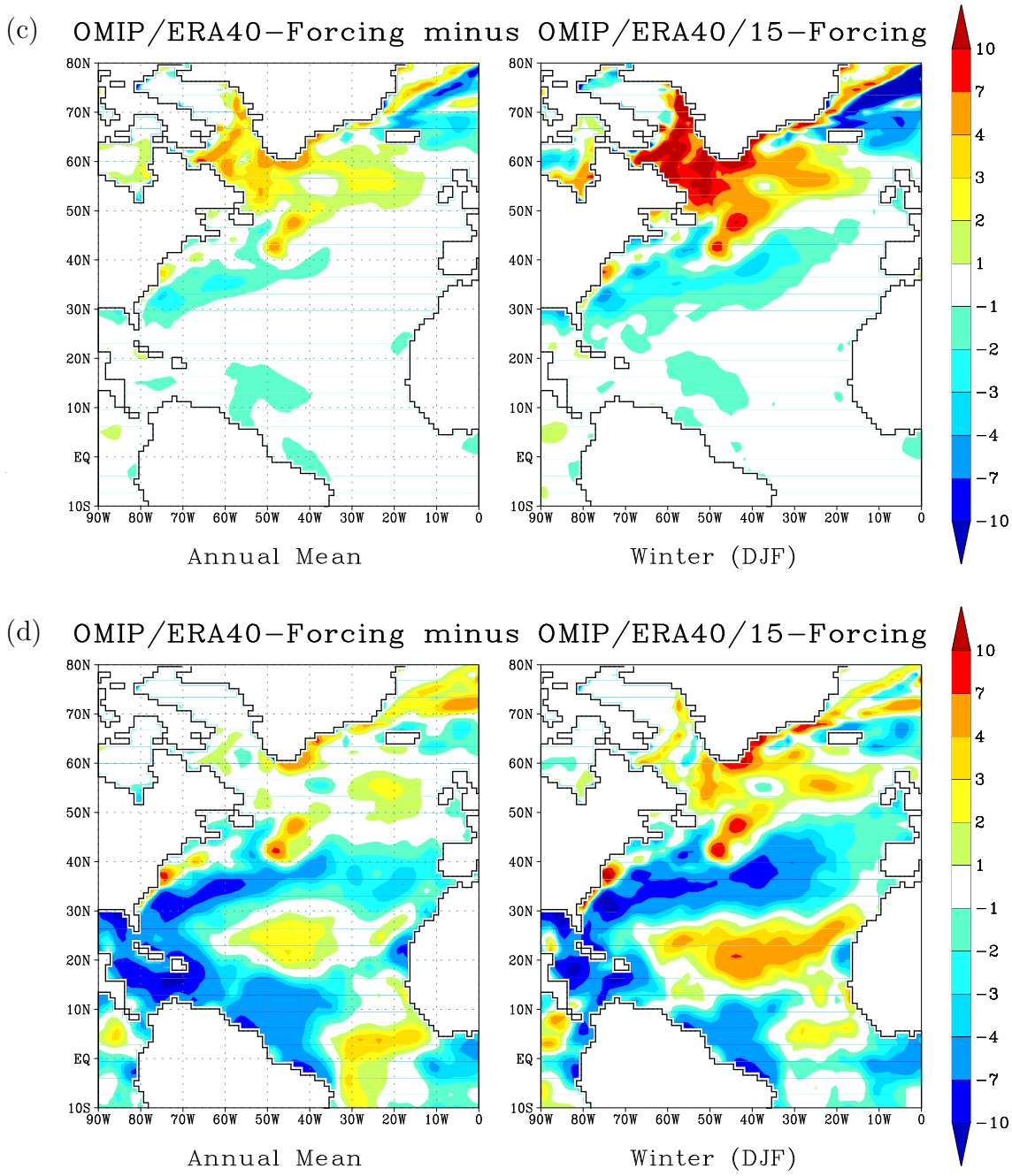

Figure 9: continued.

5 Conclusion

A global heat and fresh water dataset based on the data of the second ECMWF Re-Analysis project (ERA-40; Simmons and Gibson, 2000) is presented which is constructed in the same way as the dataset based on the data of the first project (ERA-15; Gibson et al., 1997; ROM). The datasets can be used as surface boundary conditions for global ocean/sea-ice models. These conditions are based on bulk formulae. The formulae of Kara et al. (2005) extended by a parameterization of sea ice concentration (ROM) were used. A mean annual cycle on a daily basis was constructed from ERA-40 for all relevant parameters including wind stress. Continental runoff is considered by using the runoff model of ROM.

To estimate implied meridional oceanic heat transports (Appendix D) and to avoid temporal drifts of globally averaged deep ocean temperature and salinity in ocean/sea-ice models, the heat and fresh water budgets have been closed by applying an inverse procedure after Isemer et al. (1989) and da Silva et al. (1994) to fine-tune the fluxes towards observed transports. The winds and the short wave radiation at Southern higher latitudes were corrected. For the wind correction, the global scheme from ROM was applied. Beyond this correction, short and long wave radiation were corrected in the subsidence zones by using another global scheme from ROM.

Applied to any ocean/sea-ice model and assuming a surface layer thickness of 10 m, the forcing dataset would induce a globally averaged net sea-surface buoyancy loss of only 0.006 kg m^{-3} per year.

The differences between the mean annual cycles of the ERA-40 and ERA-15 based forcing datasets are influenced by changes in the assimilation system of ERA and by effects of the different periods, as well. To separate these effects, another forcing dataset was introduced based on those data of ERA-40 covering only the ERA-15 period. The differences due to changes in the assimilation system of ERA are larger than the differences due to the different periods. The latter differences show a southward shift of the Intertropical Convergence Zone (ITCZ) in time and a pattern in the net heat flux in the North Atlantic Ocean that resembles the pattern of a low phase of the

North Atlantic Oscillation (NAO). This pattern is essentially determined by a similar pattern in the latent heat flux. The gradient in this flux across the North American Basin is about 15 to 20 Wm^{-2} for the annual mean and about 20 Wm^{-2} in winter. Therefore, the assumptions are confirmed that the dataset based on ERA-15 is biased towards a high phase of the NAO and that the dataset based on ERA-40 covers a whole NAO period.

Acknowledgements

The author would like to thank the Max-Planck-Institute for Meteorology (MPI) and the German Climate Computing Center for the possibility to carry out this work. Many thanks are owed to J. Marotzke (MPI) for financial support. The author is very grateful to A. J. Wallcraft and especially to A. Birol Kara (both U.S. Naval Research Laboratory) who kindly provided their code. The author would like to thank F. Toussaint (MPI) who provided the ECMWF Re-Analysis (ERA-40) data. NCEP Re-Analysis data were provided by the NOAA-CIRES Climate Diagnostics Center, Boulder, Colorado, USA, and obtained from their Web site at http://www.cdc.noaa.gov/. Bootstrap Sea Ice Concentrations from Nimbus-7 SMMR and DMSP SSM/I, were obtained from the EOSDIS NSIDC Distributed Active Archive Center (NSIDC DAAC), University of Colorado at Boulder. The author is grateful to A. M. da Silva who provided the data of the Atlas of Surface Marine Data on the Web site at http://ingrid.ldgo.columbia.edu:81/SOURCES/.DASILVA/.SMD94/ from where the data were obtained. The author would also like to thank K. Lohmann, J. Jungclaus, and E. Maier-Reimer for specific comments that improved the readability of the manuscript. The author thanks J. Bader for discussions. Soli Deo Gloria.

Appendix A

Net downward heat flux Q_{net} and net fresh water flux F were computed as follows:

$$\begin{aligned} Q_{net} &= p_{sw} \cdot Q_{sw} + p_{lw} \cdot Q_{lw} + p_{se} \cdot Q_{se} + p_{la} \cdot Q_{la} \\ F &= p_{pr} \cdot P + p_{la} \cdot E + p_{ru} \cdot R \end{aligned} \tag{4}$$

with

$$\begin{aligned} Q_{sw} &: \text{Short wave solar radiation} \\ Q_{lw} &: \text{Long wave radiation} \\ Q_{se} &: \text{Sensible heat flux} \\ Q_{la} &: \text{Latent heat flux} \\ P &: \text{Precipitation} \\ E &: \text{Evaporation} \\ R &: \text{Continental Runoff} \end{aligned}$$

and p_{sw}, p_{lw}, p_{se}, p_{la}, p_{pr}, and p_{ru} are the tuning parameters of the inverse procedure (Table 3 in section 3.2). If Q_{net} and F are calculated independently of the inverse procedure, then $p_i = 1$.

Q_{sw}, Q_{lw} and P are directly provided by ERA-40. R is calculated from P and E over the continents as directly provided by ERA-40 by using the runoff model from ROM. Q_{la} and Q_{se} are computed as follows: T_s is the surface temperature and T_f the freezing temperature with

$$T_f = 0.0528 - 0.0564 \cdot S \tag{5}$$

T_f is in °C. S is salinity (Levitus et al. 1994). This equation is used if salinity data are available. If not, then $T_f = -1.89$°C.

In the case $T_s > T_f$, then Q_{se} and Q_{la} are given by:

$$\begin{aligned} Q_{se} &= \rho_a c_{p,air} V c_{se} (T_a - T_s) \\ Q_{la} &= \rho_a L_w(T_s) V c_{la} (q_a - q_s) \end{aligned} \tag{6}$$

In the other case $T_s \leq T_f$, then the formulae read:

$$\begin{aligned} Q_{se} &= \rho_a c_{p,air} V (c_{se}(T_a - T_s) c_{ice} + c_{se,w}(T_a - T_f)(1 - c_{ice})) \\ Q_{la} &= \rho_a V (L_{ice} c_{la} (q_a - q_{ice}) c_{ice} + L_w(T_f) c_{la,w} (q_a - q_f)(1 - c_{ice})) \end{aligned} \tag{7}$$

ρ_a is the air density with

$$\rho_a = \frac{p}{R_{gas} T_a (1 + 0.61 q_a)} \tag{8}$$

where $R_{gas} = 287.1$ J kg^{-1} K^{-1} is the gas constant for dry air and p is the air pressure. $c_{p,air} = 1004.67$ J kg^{-1} K^{-1} is the specific heat of dry air, V is the scalar wind, T_a is the air temperature, c_{ice} is the sea ice concentration,

$$L_w = (2.501 - 0.00237 \cdot T) \cdot 10^6 \tag{9}$$

is the latent heat of vaporization in J kg^{-1}. T may be T_s as in Eq.(6) or T_f as in Eq.(7). $L_{ice} = 2.834 \cdot 10^6$ J kg^{-1} is the latent heat of sublimation.

$$\begin{array}{rcl} q_a & = & q(e_w(T_d)) \\ q_s & = & 0.9815 \cdot q(e_w(T_s)) \\ q_{ice} & = & q(e_{ice}(T_s)) \\ q_f & = & q(e_{ice}(T_f)) \end{array} \tag{10}$$

are the specific humidities with T_d is the dew point temperature and

$$q = \frac{0.62197 e}{p - 0.378 e}, \tag{11}$$

where e is the water vapor pressure which is computed by using formulae after Buck (1981):

$$\left\{ \begin{array}{c} e_w \\ e_{ice} \end{array} \right\} = a \cdot e^{\left[\frac{(b - T/d)T}{T + c} \right]} \tag{12}$$

with the coefficients a,b,c, and d as in Table 6. In (10) only $e_w(T_d)$ is not saturated, all other combinations of e_w and e_{ice} are saturated ones.

c_{se}, $c_{se,w}$, c_{la}, $c_{la,w}$ are the transfer coefficients after Kara et al. (2005) with

$$\begin{array}{rcll} c_{se} & = & 0.9554 & c_{la} \\ c_{se,w} & = & 0.9554 & c_{la,w} \end{array} \tag{13}$$

c_{la} is a function of $T_a - T_s$ and V and $c_{la,w}$ is a function of $T_a - T_f$ and V. The FORTRAN90 code for calculating the turbulent heat fluxes is available

condition	a	b	c	d
water (e_w)	6.1121	18.729	257.87	227.3
ice (e_{ice})	6.1115	23.036	279.82	333.7

Table 6: Coefficients to calculate the water vapor pressure (hPa) of pure water as a function of temperature (°C).

at http://www.omip.zmaw.de/omip/forcing365/bulk_formulae/turbhf.f90 including the code for computing the transfer coefficients after Kara et al. (2005) who call them Naval Research Laboratory Air-Sea Exchange Coefficients (NASEC; http://www7320.nrlssc.navy.mil/nasec/nasec.html).

Over the oceans, evaporation E is computed from the latent heat flux Q_{la} with

$$\begin{aligned} E &= Q_{la}/L_w/10^3 \qquad if \quad T_s > T_f \\ E &= Q_{la}/L_{ice}/10^3 \qquad if \quad T_s \leq T_f. \end{aligned} \tag{14}$$

Appendix B

A global scheme is presented which can be applied to correct, i.e. to increase the winds off the Antarctic coast. Because the turbulent heat fluxes are a function of the scalar wind, the scheme is based only on the scalar winds and not on the vectorial winds from ERA. From the ERA land-sea mask two coastlines were derived, one using grid points where land is defined and another coastline using grid points where water is defined. For a given grid point of the land coastline the neighboring grid point of the sea coastline was searched for. The scalar winds on these pairs of grid points are compared with each other. Normally, one would expect that winds over the oceans are larger than over the continents, because the roughness over the oceans is much smaller. Therefore, it is hypothesized that if the wind on the sea coastline u_{sea} is smaller than the wind on the land coastline u_{land}, something went wrong in the ECMWF model and u_{sea} should be corrected, i.e. increased. Such a correction should be proportional to the difference of the winds. However,

the winds on the land coastline are underpredicted by an atmosphere model of the same resolution as ERA have (van den Broeke and van de Wal, 1997). Therefore, the correction should be extended by a proportionality factor c_u:

$$\delta u = (u_{land} - u_{sea}) \cdot c_u \cdot d \tag{15}$$

In this scheme no Coriolis effect is included which deflects the offshore winds to the west off the Antarctic coast whereby strong easterlies around this continent are formed (Davis and McNider 1997). Their katabatic wind model suggested a decrease of the wind speed with increasing distance from the coast. Therefore, δu is only applied up to a maximum distance from the coast of four grid points with a factor d which decreases linearly from 1 to 0.5. c_u was adjusted such that the peak of the corrected zonally averaged winds was slightly smaller than the peak of the strong westerlies at 50°S ($c_u = 15$) (Fig.10) following the figure of zonally averaged wind stress in Gill (1982) (Davis and McNider 1997). Equation (15) was applied only if $T_a(°C) < 0$ with T_a the 2 meter air temperature. Only annual mean scalar winds and temperatures were used.

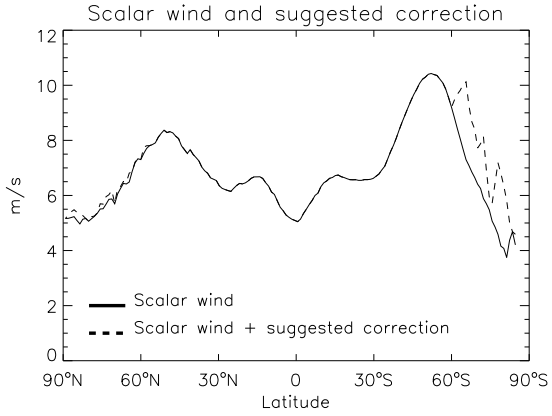

Figure 10: Zonally averaged scalar wind of ERA and suggested by the wind correction model.

The main effects of this scheme are off Antarctica (Fig.10). There are also effects off Northern Greenland but they are comparably small. Because

the two-dimensional distribution of the correction is not realistic in detail, only a qualitative description is given here. The scheme shows effects over the coastal seas at almost whole East Antarctica: Princess Ragnhild Coast, West Ice Shelf, Shackleton Ice Shelf, and Adelie Coast. Furthermore, there are also effects near West Antarctica, the Getz Ice Shelf, and in the Weddell sea, the Filchner Ice Shelf.

Appendix C

A global scheme is presented to correct, i.e. to reduce the short and long wave radiations from ERA in the regions of subsidence of the Walker cell. The idea for this scheme was inspired by a statistical analysis of the ERA data by Oberhuber (1999). He observed a dependence of short wave radiation on cloudiness to the power of four:

$$\kappa = \frac{1}{1 + 2.8(1 + e^2)n^4} \tag{16}$$

with n is the cloudiness and e is the water vapor pressure with

$$e = 6.11 \cdot 10^{7.5\frac{T_d - 273.16}{T_d - 35.86}} \tag{17}$$

with T_d is the dew point temperature. By using κ, a correction ΔQ_{sw} to be subtracted from the short wave radiation Q_{sw} can be calculated as follows:

$$\Delta Q_{sw} = Q_{sw}(1 - Min(\frac{\mu}{\bar{\mu}}, 1)) \tag{18}$$

with

$$\mu = \frac{1}{1 + 0.5\kappa} \tag{19}$$

and $\bar{\mu}$ is the global average of μ.

A similar correction for the long wave radiation can be obtained by replacing equations (16) and (17) with

$$\kappa = 1 - (0.51 + 0.4\frac{|\phi|}{90^\circ})n^2 \tag{20}$$

with n again is cloudiness and ϕ is the latitude, following the formula of Clark (1974) (Josey et al. 1997). A correction ΔQ_{lw} to be subtracted from the long wave radiation Q_{lw} can be computed as follows:

$$\Delta Q_{lw} = (Q_{lw} - 4\varepsilon\sigma T_s^3(T_s - T_a))(1 - Min(\frac{\mu}{\bar{\mu}}, 1)) \tag{21}$$

with $\varepsilon = 0.97$ is the emissivity of water, $\sigma = 5.67 \cdot 10^{-8}$ $\mathrm{Wm^{-2}K^{-4}}$ is the Stefan-Boltzmann constant, and μ as in equation (19) and $\bar{\mu}$ as above. The correction should be applied only on that part of Q_{lw} affected by clouds. Therefore, assuming Q_{lw} can be approximated roughly by the formula after Clark (1974), the term without cloudiness is subtracted before. For this scheme the daily data of the mean annual cycle were used.

Appendix D

The implied meridional oceanic heat and fresh water transports are defined as follows: Let $f(\lambda, \phi, \mathbf{p})$ be the net heat flux Q_{net} or fresh water flux F (Appendix A). Then the meridional heat or fresh water transport $T(\phi, \mathbf{p})$ is calculated as:

$$T(\phi, \mathbf{p}) = \int_{northpole}^{\phi} d\phi' \int_{\lambda_{west}}^{\lambda_{east}} f(\lambda, \phi', \mathbf{p}) d\lambda \tag{22}$$

Here, λ_{west} and λ_{east} are determined by the basin chosen: Atlantic, Pacific, and Indian Ocean, as well as the global ocean.

Appendix E

Buoyancy B is computed with B following Oberhuber (1988):

$$B = g\left(\frac{\alpha}{c_{p,water}\rho} Q_{net} - \beta SF\right) \tag{23}$$

with Q_{net} and F as in Appendix A and $g = 9.8\mathrm{m\ s^{-2}}$ is the gravitational constant, $c_{p,water} = 4180$ J $\mathrm{kg^{-1}}$ $\mathrm{K^{-1}}$ is the specific heat of water, ρ is the

density of water by using the UNESCO formula (1983) for the equation of state of sea water, and S is salinity (Levitus, 1994). The thermal expansion coefficient α and the haline contraction coefficient β are defined by:

$$\begin{aligned} \alpha &= \frac{1}{\rho}\frac{\partial \rho}{\partial T}\Big|_{P,S} \\ \beta &= \frac{1}{\rho}\frac{\partial \rho}{\partial S}\Big|_{P,T}. \end{aligned} \tag{24}$$

Note that α is negative and β is positive. These derivatives were calculated numerically by using $\Delta T = 0.01$K and $\Delta S = 0.01$.

References

van den Broeke, M.R. and R.S.W. van de Wal, 1997. Representation of Antarctic Katabatic Winds in a High-Resolution GCM and a Note on Their Climate Sensitivity. Journal of Climate, Vol. 10, pp.3111-3130.

Buck, A.L., 1981. New Equations for Computing Vapor Pressure and Enhancement Factor. Journal of Applied Meteorology, Vol.20, pp.1527-1532.

Clark, N.E., L.Eber, R.M.Laurs, J.A.Renner, and J.F.T.Saur (1974) Heat exchange between ocean and atmosphere in the eastern North Pacific for 1961-71, NOAA Tech. Rep. NMFS SSRF-682, U.S.Dep.of Commer., Washington, D.C.

Comiso, J. (1999), updated (2002). Bootstrap sea ice concentrations for NIMBUS-7 SMMR and DMSP SSM/I, June to September 2001. Boulder, CO, USA: National Snow and Ice Data Center. Digital media.

da Silva, A.M., C.C.Young and S.Levitus, 1994. Atlas of surface marine data, Vol.1-5, NOAA Atlas NESDIS 6-10.

Davis, A.M.J. and R.T.McNider (1997) The Development of Antarctic Katabatic Winds and Implications for the Coastal Ocean. Journal of the Atmo-

spheric Sciences, Vol.54, pp.1248-1261.

Fairall, C. W., Bradley, E. F., Hare, J. E., Grachev, A. A., Edson, J. B., 2003: Bulk Parameterization of Air-Sea Fluxes: Updates and Verification for the COARE Algorithm. J. Climate 16, 571-591.

Fritzsch, B., R. Gerdes, W. Hiller, M. Latif, S. Legutke, E. Maier-Reimer, D. Olbers, F. Röske, 2000. The Ocean Model Intercomparison Project. Vergleich der thermohalinen Zirkulation in zwei globalen ozeanischen Zirkulationsmodellen by the German OMIP Group. Bericht des Alfred-Wegener-Instituts für Polar- und Meeresforschung, Bremerhaven (http://www.omip.zmaw.de/omip/omip_report.php).

Fritzsch, B., R. Johanni, C. Köberle, 1998. Parallelization of a global ocean circulation model with coupled sea ice. Proceedings Fourth European SGI/ CRAY MPP Workshop (H. Lederer, F. Hertweck, eds.). Garching, 1998, 133-139.

Garnier, E., B.Barnier, L.Siefridt and K.Béranger, 2000. Investigating the 15 years air-sea flux climatology from the ECMWF Re-Analysis project as a surface boundary condition for ocean models. International Journal of Climatology, 20, 1653-1673 (2000).

Gibson, J.K., P.Kallberg, S.Uppala, A.Hernandez, A.Nomura, E.Serrano, 1997. ECMWF Re-Analysis, Project Report Series, 1.ERA Description. European Centre for Medium-Range Weather Forecasts, Reading, England.

Grist, J. P. and S. A. Josey, 2003. Inverse Analysis of the SOC Air-Sea Flux Climatology Using Ocean Heat Transport Constraints, Journal of Climate, 16(20), 3274-3295.

Haak, H., J.Jungclaus, U.Mikolajewicz, and M. Latif, 2003. Formation and

propagation of great salinity anomalies. Geophysical Research Letters, Vol. 30, No.9, 1473, doi:10.1029/2003GL017065.

Hagemann, S. and L. Dümenil, 1998. A parametrization of the lateral waterflow for the global scale. Climate Dynamics 14 (1), pp. 17-31.

Hagemann, S., Arpe, K., and Bengtsson, L., 2005. Validation of the hydrological cycle of ERA40. Report on Earth System Science No.10, Max-Planck-Institut für Meteorologie, Hamburg, Germany.

Isemer, H.-J., J. Willebrand, and L. Hasse, 1989. Fine Adjustment of Large Scale Air-Sea Energy Flux Parameterizations by Direct Estimates of Ocean Heat Transport. Journal of Climate, Vol.2, pp.1173-1184.

Johns,W.E., T.N.Lee, R.J.Zantopp, and E.Fillenbaum, 1997. Updated Transatlantic Heat Flux at 26.5°N. WOCE Newsletter No.27, pp.15-22.

Josey, S.A., D.Oakley, and R.W.Pascal (1997) On estimating the atmospheric longwave flux at the ocean surface from ship meteorological reports. Journal of Geophysical Research, Vol.102, No.C13, pp.27961-27972.

Kalnay, E., Kanamitsu, M., Kistler, R., Collins, W., Deaven, D., Gandin, L., Iredell, M., Saha, S., White, G., Woollen, J., Zhu, Y., Chelliah, M., Ebisuzaki, W., Higgins, W., Janowiak, J., Mo, K.C., Ropelewski, C., Wang, J., Leetmaa, A., Reynolds, R., Jenne, R., Joseph, D., 1996. The NCEP/ NCAR 40-Year Reanalysis Project, Bulletin American Meteorological Society, 77(3), 437-470.

Kara, A. B., H. E. Hurlburt, A. J. Wallcraft, 2005. Stability-dependent exchange coefficients for air-sea fluxes. J. Atmos. Oceanic Technol., 22, 1077-1091.

Keith, D.W., 1995. Meridional energy transport: uncertainty in zonal means. Tellus 47A, 30-44.

Kim, S.-J. and A. Stössel, 1998. On the representation of the Southern Ocean water masses in an ocean climate model. Journal of Geophysical Research, Vol. 103, No. C11, pp.24891-24906.

Lebedev, K.V. and M.I.Yaremchuk (2000) A diagnostic study of the Indonesian Throughflow. Journal of Geophysical Research, Vol.105, No. C5, p.11243-11258.

Levitus, S., R. Burgett and T. Boyer (1994) World Ocean Atlas, 1994, Volume 3, Salinity. NOAA Atlas NESDIS 3.

Macdonald, A.M. (1993) Property Fluxes at 30°S and Their Implications for the Pacific-Indian Throughflow and the Global Heat Budget. Journal of Geophysical Research, Vol.98, No. C4, pages 6851-6868.
Macdonald, A.M. and C. Wunsch, 1996. Oceanic Estimates of Global Ocean Heat Transport. international WOCE Newsletter, No.24, pp.5-6, Oct. 1996.

Oberhuber, J.M., 1988. An Atlas Based on the 'COADS' Data Set: The Budgets of Heat, Buoyancy and Turbulent Kinetic Energy at the Surface of the Global Ocean. Report No.15, Max-Planck-Institut für Meteorologie, Hamburg.

Oberhuber, J.M., 1999. Description of the Parallel Isopycnal Primitive Equation OGCM, PIPE. Deutsches Klimarechenzentrum, Modelle & Daten, Technical Report No.19, Hamburg.

Pacanowski, R., C., 1995. MOM 2, Documentation, User's Guide and Reference Manual, Version 1.0. GFDL Ocean Technical Report No.3, Princeton, 232 pp.

Röske, F., 2001. An atlas of surface fluxes based on the ECMWF Re-Analysis - a climatological dataset to force global ocean general circulation models. Report No.323, Max-Planck-Institut für Meteorologie, Hamburg, Germany.

Röske, F., 2006. A Global Heat and Freshwater Forcing Dataset for Ocean Models. Ocean Modelling, Volume 11, Issues 3-4, Pages 235-297.

Simmons, A. J. and J. K. Gibson, 2000. The ERA-40 Project Plan, ERA-40 Project Report Series, 1, 63pp, ECMWF, Shinfield Park, Reading, UK.

Trenberth, K.E. and J.M.Caron, 2001. Estimates of Meridional Atmosphere and Ocean Heat Transports. Journal of Climate, Vol.14, pp.3433-3443.

UNESCO, 1983. Algorithms for computation of fundamental properties of seawater. Unesco technical papers in marine science 44.

Wanner, H., S. Brönnimann, C. Casty, D. Gyalistras, J. Luterbacher, C. Schmutz, D. B. Stephenson, E. Xoplaki, 2001. North Atlantic Oscillation - Concepts and Studies. Surveys in Geophysics, 22: 321 - 382.

Wolff, J.-O., E. Maier-Reimer, and S. Legutke, 1997: The Hamburg Ocean Primitive Equation Model. Technical report, No.13, German Climate Computer Center (DKRZ), Hamburg, 98 pp.

Woodruff, S.D., R.J.Slutz, R.L.Jenne, and P.M.Steurer, 1987. A comprehensive ocean-atmosphere data set. Bulletin American Meteorological Society, Vol.68, No.10, 1239-1250.

Woodruff, S.D., S.J.Lubker, K.Wolter, S.J.Worley and J.D.Elms, 1993. Comprehensive Ocean-Atmosphere Data Set (COADS) release 1a: 1980-92. Earth System Monitor, 4 (1), 4-8.

MPI-Examensarbeit-Referenz:

Examensarbeit Nr. 1-82 bei Bedarf bitte Anfragen:
MPI für Meteorologie, Abtlg.: PR, Bundesstr. 53, 20146 Hamburg

Examensarbeit Nr. 83 Juli 2001	**Aggregate models of climate change: development and applications** Kurt Georg Hooss
Examensarbeit Nr. 84 Februar 2002	**Ein Heterodyn-DIAL System für die simultane Messung von Wasserdampf und Vertikalwind: Aufbau und Erprobung** Stefan Lehmann
Examensarbeit Nr. 85 April 2002	**Der Wasser- und Energiehaushalt der arktischen Atmosphäre** Tido Semmler
Examensarbeit Nr. 86 April 2002	**Auswirkungen der Assimilation von Meereshöhen-Daten auf Analysen und Vorhersagen von El Niño** Sigrid Schöttle
Examensarbeit Nr. 87 Juni 2002	**Atmospheric Processes in a young Biomass Burning Plume - Radiation and Chemistry** Jörg Trentmann
Examensarbeit Nr. 88 August 2002	**Model Studies of the Tropical 30 to 60 Days Oscillation** Stefan Liess
Examensarbeit Nr. 89 Dezember 2002	**Influence of Sub-Grid Scale Variability of Clouds on the Solar Radiative Transfer Computations in the ECHAM5 Climate Model** Georg Bäuml
Examensarbeit Nr.90 Mai 2003	**Model studies on the response of the terrestrial carbon cycle to climate change and variability** Marko Scholze
Examensarbeit Nr.91 Juni 2003	**Integrated Assessment of Climate Change Using Structural Dynamic Models** Volker Barth
Examensarbeit Nr.92 Juli 2003	**Simulations of Indonesian Rainfall with a Hierarchy of Climate Models** Edvin Aldrian
Examensarbeit Nr.93 Juli 2003	**ENSO Teleconnections in High Resolution AGCM Experiments** Ute Merkel
Examensarbeit Nr.94 Juli 2003	**Application and Development of Water Vapor DIAL Systems** Klaus Ertel

MPI-Examensarbeit-Referenz:

Examensarbeit Nr. 1-82 bei Bedarf bitte Anfragen:
MPI für Meteorologie, Abtlg.: PR, Bundesstr. 53, 20146 Hamburg

Beginn einer neuen Veröffentlichungsreihe des MPIM, welche die vorherigen Reihen "Reports" und "Examensarbeiten" weiterführt:

„Berichte zur Erdsystemforschung" , „*Reports on Earth System Science*", ISSN 1614-1199
Sie enthält wissenschaftliche und technische Beiträge, inklusive Dissertationen.

Berichte zur Erdsystemforschung Nr.1 Juli 2004	**Simulation of Low-Frequency Climate Variability in the North Atlantic Ocean and the Arctic** Helmuth Haak
Berichte zur Erdsystemforschung Nr.2 Juli 2004	**Satellitenfernerkundung des Emissionsvermögens von Landoberflächen im Mikrowellenbereich** Claudia Wunram
Berichte zur Erdsystemforschung Nr.3 Juli 2004	**A Multi-Actor Dynamic Integrated Assessment Model (MADIAM)** Michael Weber
Berichte zur Erdsystemforschung Nr.4 November 2004	**The Impact of International Greenhouse Gas Emissions Reduction on Indonesia** Armi Susandi
Berichte zur Erdsystemforschung Nr.5 Januar 2005	**Proceedings of the first HyCARE meeting, Hamburg, 16-17 December 2004** Edited by Martin G. Schultz
Berichte zur Erdsystemforschung Nr.6 Januar 2005	**Mechanisms and Predictability of North Atlantic - European Climate** Holger Pohlmann
Berichte zur Erdsystemforschung Nr.7 November 2004	**Interannual and Decadal Variability in the Air-Sea Exchange of CO2 - a Model Study** Patrick Wetzel
Berichte zur Erdsystemforschung Nr.8 Dezember 2004	**Interannual Climate Variability in the Tropical Indian Ocean: A Study with a Hierarchy of Coupled General Circulation Models** Astrid Baquero Bernal
Berichte zur Erdsystemforschung Nr9 Februar 2005	**Towards the Assessment of the Aerosol Radiative Effects, A Global Modelling Approach** Philip Stier
Berichte zur Erdsystemforschung Nr.10 März 2005	**Validation of the hydrological cycle of ERA40** Stefan Hagemann, Klaus Arpe and Lennart Bengtsson
Berichte zur Erdsystemforschung Nr.11 Februar 2005	**Tropical Pacific/Atlantic Climate Variability and the Subtropical-Tropical Cells** Katja Lohmann
Berichte zur Erdsystemforschung Nr.12 Juli 2005	**Sea Ice Export through Fram Strait: Variability and Interactions with Climate** Torben Königk


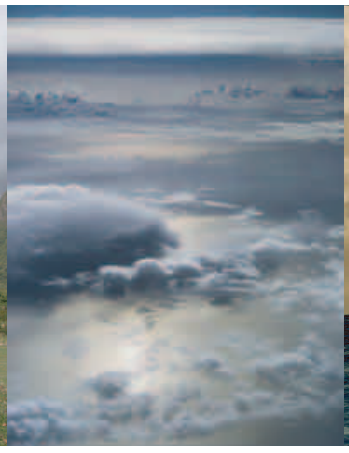


ISSN 1614-1199